4

Microfluidic Tools for the Synthesis of Bespoke Quantum Dots

Shangkun Li, Jeff C. Hsiao, Philip D. Howes, and Andrew J. deMello

ETH Zürich, Institute of Chemical and Bioengineering, Vladimir-Prelog-Weg 1-5/10, 8093 Zurich, Switzerland

4.1 Introduction

4.1.1 Microfluidics in the Chemical and Biological Sciences

Microfluidic systems are now pervasive in almost all areas of experimental science, with interest in this technology set being driven by concomitant developments in fields such as genomics, proteomics, single-cell analysis, drug discovery, high-throughput screening, and diagnostics. In simple terms, microfluidic systems are engineered fluidic devices where flow is nonturbulent and thus highly ordered. Normally, this coincides with critical dimensions of device features on the order of tens to hundreds of microns. Such devices are adept at manipulating small volumes of fluids (10^{-9} to 10^{-18} l) within complex fluidic networks, with their use affording rapid and efficient experimentation in both the chemical and biological arena [1–5]. In specific regard to molecular synthesis, microfluidic tools have been highly successful in defining new instrumental platforms that are able to efficiently manipulate, process, and analyze molecular reactions on micrometer to nanometer scales [6–9]. The primary reason why microfluidic systems provide unique environments for performing synthesis is the dependency of fluid flow characteristics on scale. The atypical fluid behavior in small-volume environments directly leads to a number of key features. These include the ability to process miniscule volumes of sample and reagents, efficient mass and thermal transport, precise and dynamic control of reaction parameters (such as temperature, reaction time, and reagent concentrations), and the ability to integrate a range of optical tools to probe reactions in a sensitive and real-time manner. All of these features provide the experimentalist with a unique opportunity to perform a synthetic process in a rapid, high-throughput, efficient, and controllable manner.

4.1.2 Compound Semiconductor Nanoparticles

Recent years have seen the discovery of a range of novel properties, processes, and phenomena at the nanoscale. Such discoveries have generated revolutionary opportunities for creating novel materials and devices with superior chemical,

Nanotechnology and Microfluidics, First Edition. Edited by Xingyu Jiang.

physical, and biological characteristics. Nanocrystalline materials are of special interest in this regard owing to their tunable physical and chemical properties and their potential utility as functional elements in biological experimentation, optoelectronics, optical communications, and laser technologies. Semiconductor nanoparticles (NPs) or quantum dots (QDs) are nanometer-scale crystallites possessing radii smaller than the exciton Bohr radius. This property engenders unique quantum effects, such as quantum confinement and macroscopic quantum tunneling, which are not present in the bulk crystallite [10, 11]. Accordingly, by controlling their composition, shape, and size, QDs can be made to exhibit tunable broadband emission within the ultraviolet (UV), visible, and near-infrared (NIR) regions of the electromagnetic spectrum [12]. As illustrated schematically in Figure 4.1, the band gap (defined as the minimum energy needed to excite an electron from the valence band to the conduction band) of a QD decreases as a function of particle size. This means that smaller QDs require more energy to be excited, with higher energy (lower wavelength) photons being released when the QDs return to their ground electronic state [13], resulting in a blue to red emission shift with QD size. Such unique optoelectronic properties

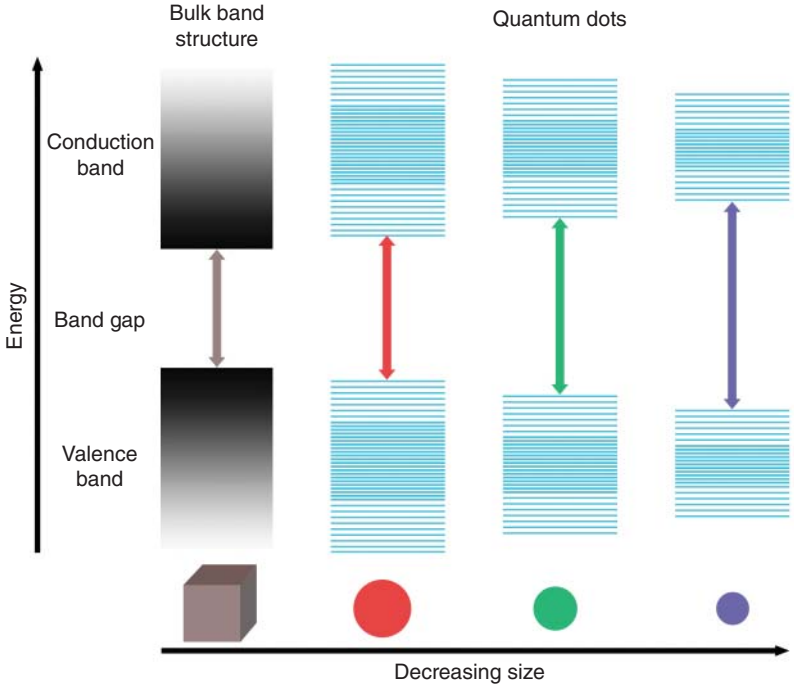

Figure 4.1 Schematic illustration of the dependence of the electronic band gap on particle size in bulk crystallites and QDs. As the size of the crystal decreases, the difference in energy between the highest valence and the lowest conduction band increases. Accordingly, QDs can emit a range of wavelengths from the same material as a function of their size. In this way, it is possible for their optical and electronic properties to be adjusted as needed.

make QDs enormously promising materials for a wide range of sensing [14, 15], display [16–18], and bioimaging [19–21] applications.

In the late 1980s, QDs based on elements in groups II–VI of the periodic table (i.e. II–VI, III–V, and IV–VI materials) were synthesized in a bottom-up manner to study size quantization effects [22, 23]. Since then, a great variety of QD compositions and structures have been realized and investigated. These include core-type QDs such as cadmium selenide (CdSe) and lead sulfide (PbS), core/shell QDs such as CdS/ZnSe (cadmium sulfide/zinc selenide) and CdSe/CdS, and core/multishell QDs such as CdSe/CdS/ZnS (zinc sulfide) [24–27]. To ensure the facile synthesis of high-quality QDs with tunable physical and chemical properties, significant efforts have been devoted to developing robust synthetic methodologies over the past three decades. Generally, bottom-up techniques for QD synthesis involve vapor-phase epitaxial growth or wet-chemical methods [28]. In vapor-phase synthesis, QDs are grown through epitaxial self-assembly by deposition onto the surface of a semiconductor layer. Vapor-phase grown QDs have high crystallinity and low defect densities; however, this method is hampered by the need for sophisticated instrumentation and the difficulties associated with separating synthesis products from the substrate [29]. Accordingly, liquid-phase synthesis procedures, whose origins can be traced back to the synthesis of gold colloids by Faraday in the 1850s [30], are most commonly used. Such methods in principle provide for the controlled nucleation and growth of NPs within a solution of chemical precursors containing both metal and anion sources [31].

Classical nucleation theory was transferred to liquid-phase NP synthesis by LaMer and Dinegar in the 1950s, through the concept of burst nucleation [32]. The so-called "LaMer model" of NP nucleation and growth is highly constructive in understanding the mechanism behind colloidal NP formation [32]. As shown schematically in Figure 4.2, NPs can be considered to form via a two-stage process. An initial nucleation stage, where seed particles spontaneously precipitate from solution, is followed by a more gradual growth phase where diffusion of solutes from the solution to the seed surface proceeds until the desired particle size is attained. In physical terms, as the reaction proceeds, the solute concentration will at some point exceed a "supersaturation" concentration, eventually reaching a "critical" concentration at which time nucleation occurs. Nucleation is ideally a transient process and leads to a partial reduction of the supersaturation concentration. Once the solute concentration is lower than the nucleation concentration, the nucleation stage terminates and the residual supersaturated solute is depleted by NP growth. During the growth phase, the overall free energy of the system decreases until all solute has been consumed. Finally, NP aggregation occurs over a much longer timescale and acts to reduce the free energy of the system further. In the context of QD synthesis, aggregation is almost always undesirable, as it leads to polydispersity and flocculation/precipitation of the synthesized NPs.

In conventional macroscale reactors, nucleation and growth often occur concurrently because of poor thermal transfer, uneven mixing, and slow mass transfer. This state of affairs results in a broad-size distribution of the final product population. Significant variations in the physical environment across macroscale

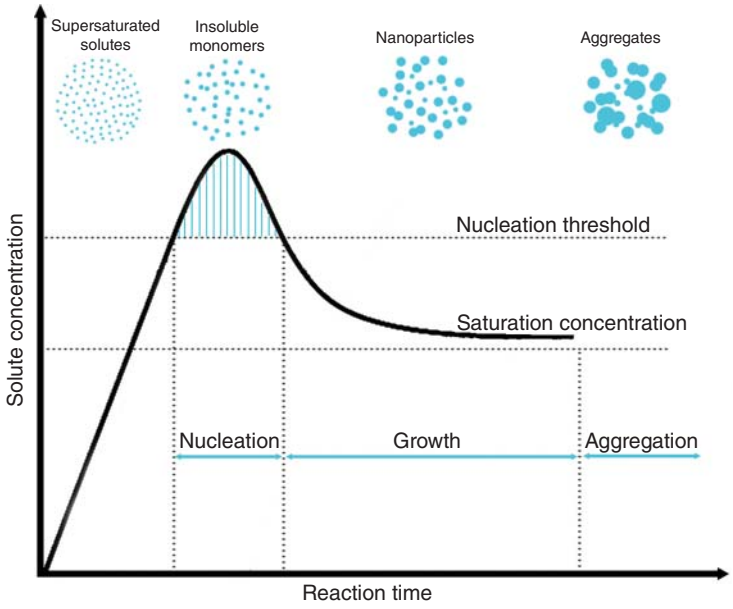

Figure 4.2 The LaMer model describing nanoparticle formation. The solute concentration will exceed the supersaturation concentration at some point during the reaction, and when the concentration exceeds the nucleation threshold, nucleation is initiated. During the growth phase, the overall free energy of the system decreases until all solute has been consumed. Nanoparticle aggregation occurs over a much longer timescale and acts to reduce the free energy of the system further.

reactors are almost always unavoidable. Accordingly, microfluidic systems, which are characterized by rapid and controlled thermal and mass transport, are an ideal format for NP production, offering enhanced control over the entire synthetic process [33].

4.1.3 Microfluidic Tools for Nanoparticle Synthesis

It can be argued that the first microfluidic devices were developed as early as the 1940s [34]; however, the field of microfluidics as we know it today began in the 1990s when Manz et al. introduced the concept of the miniaturized total analysis system (μTAS) [35]. After early demonstrations of chip-based analytical separations (most notably based around electrophoretic techniques [36]), the field rapidly expanded to showcase microfluidic tools for cell-based assays, small molecule synthesis, DNA analysis, high-throughput screening, and the study of living organisms [1].

The first report of a microfluidic reactor for NP synthesis was presented by Edel et al. [37]. In this pioneering study, the authors showed that continuous-flow microfluidic reactors significantly outperform macroscale systems in the direct production of nanoscale materials, with variations in reaction residence times being used to control average particle size and minimize sample size distributions. Since this first report, microfluidic reactors have become an established and even preferred method for the production of nanomaterials such as noble

metal NPs [38–40], metal oxide NPs [41–43], polymer NPs [44–46], silica NPs [47, 48], and semiconductor NPs [37, 49]. In addition to the previously listed advantages, the ability to integrate a range of functional components (such as thermal units, optical modules, precision pumps, flow controllers, and delivery modules) has ensured that microfluidic platforms provide for rapid and precise control of chemical state functions, enable characterization of QD composition and structure in real time, and allow the study of the kinetics of nanocrystal nucleation and growth [50]. Put simply, recent years have shown that microfluidic systems allow for the direct, rapid, cost-effective synthesis of bespoke nanomaterials in a manner inaccessible to traditional production methods [51].

In this chapter, we discuss three different classes of QDs: homogenous core-type, heterogenous core/shell, and heterogenous core/multishell (Figure 4.3a). We present the basic design principles and considerations

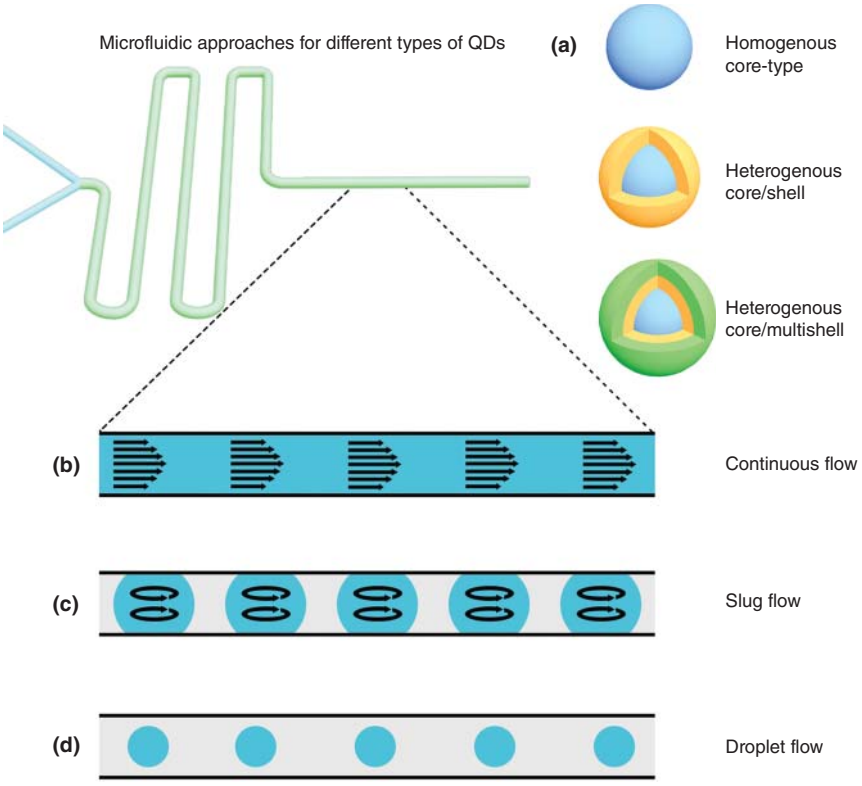

Figure 4.3 An illustration of the QD classes and the microfluidic approaches to their synthesis. (a) The different nanostructure types of QDs, including homogenous core-type, heterogenous core/shell, and heterogenous core/multishell. Illustration of (b) continuous-flow and (c, d) segmented-flow regimes in channels with circular cross sections. In a continuous flow, the fluid at the center moves faster than the fluid at the walls, resulting in a parabolic velocity profile across the channel. In a slug flow (c), an immiscible phase (gray) is injected into the channel, resulting in the reaction phase (blue) segregating into discrete slugs. In droplet flow (d), an increased amount of the immiscible phase, which preferentially wets the walls, is introduced, causing the reaction phase to become fully isolated from the channel walls.

related to the construction of microfluidic reactors for QD synthesis, followed by an explanation of the terms "continuous flow" and "segmented flow." We then discuss separately the most important and innovative advances in continuous- and segmented-flow microfluidic reactors in relation to the three classes of QDs. Finally, we speculate on potential future directions and discuss why microfluidic systems will likely continue to play a vital role in QD synthesis.

4.2 Design Considerations

Microfluidic reactors come in a number of forms, but with all embodiments leveraging scale to effect performance improvements. Microfluidic systems can be made using macroscale components, such as capillaries or tubing, or fabricated within planar chip-based substrates using conventional or soft-lithographic methods. Through the development of integrated components such as pneumatic valves, mixers, and pumps, these devices can be tailored to the specific requirements of a synthetic procedure [1]. Capillary- or tube-based reactors are much simpler in terms of design and fabrication because of the commercial availability and standardization of components (such as tubing, connectors, fittings, and valves) but are limited in their ability to perform complex procedures and plagued by excessive dead volumes. That said, capillary materials can be tailored to the experiment in question (e.g. in regard to temperature and chemical compatibility requirements) and thus have been used to fabricate a variety of high-quality nanomaterials [51]. On the other hand, chip-based microfluidic systems can incorporate highly complex fluidic networks with channel dimensions ranging on the micrometer–nanometer scale. Such systems enable the performance of more complex synthetic protocols but are more constrained in the choice of substrate materials.

At an operational level, flow-based microfluidic reactors can also be classified according to the nature of the contained fluid flow. Continuous-flow (single-phase) systems involve the continuous motivation of one or more miscible fluid streams through a microfluidic network, with mixing being controlled by diffusion orthogonal to the laminar flow [52, 53]. Such continuous-flow formats, although useful in many situations, often become impractical because of the issues related to Taylor dispersion, solute–surface interactions, cross-contamination, and the need for substantial volumes of reagents and relatively long channel lengths. Conversely, segmented-flow (or droplet-based) microfluidic systems involve the use of two immiscible phases (such as water and oil) to generate streams of droplets containing the reagents of interest. Although a variety of droplet generation mechanisms can be used, all involve the establishment of an interface between coflowing, immiscible fluids, followed by self-segregation of one of the fluids into (pl–nl sized) droplets that are surrounded by the other (continuous) fluid. Such systems are ideally suited to process millions of individual reactions on short timescales with exceptional reproducibility and have already begun to impact the development of novel high-throughput experimentation and screening platforms. We now provide a

brief discussion of both continuous-flow and droplet-based microfluidics and their utility in QD synthesis.

4.2.1 Continuous-Flow Microfluidics

Continuous-flow reactors can be considered the simplest microfluidic systems and, as noted, can be produced via the assembly of capillaries or by conventional and soft lithographic techniques. In continuous-flow systems, reagents and solvents are introduced into microchannels under laminar flow (low Reynolds' number) conditions by precision syringe pumps or by back-pressure from tubing connections. Significantly, because fluids are motivated at constant average velocities, kinetic or temporal information can be extracted through a space-to-time conversion, by measuring the product formation at different positions along the microchannel. In such reactors, product quality is influenced by reaction time, temperature, reagent concentrations, and mixing efficiency, with the final products being collected as they emerge from the reactor.

It is important to remember that control of microchannel dimensions in continuous-flow systems ensures that the desired experimental conditions are reached within milliseconds and that reagent usage is minimized. For more complex synthetic schemes, the chemical composition of the reaction mixture can also be varied by the introduction of further reagents along the reaction channel. Moreover, large-scale syntheses can be performed (for certain materials) using continuous-flow reactors by operating them for extended periods of time and leveraging the concept of scale-out [54]. Finally, continuous-flow microreactors are ideally suited for processing reactions involving unusual conditions, such as high temperatures or the presence of toxic precursors, because of the precise control of reaction parameters [55, 56].

In regard to the use of continuous-flow reactors for QD synthesis, it is important to note two issues that often limit their application. First, synthesized QD populations may often have relatively large particle-size distributions as a consequence of the nonuniform (parabolic) flow profile of the reaction mixture as the fluid moves along the microchannel (Figure 4.3b). In simple terms, the contained fluid moves faster at the center of the channel, and with a decreasing velocity, the closer it is to the channel walls, where the flow is at its slowest. This is due to viscous drag [51]. Second, the synthesized products may interact with and precipitate onto the channel surfaces, altering the hydrodynamic environment and ultimately causing permanent blockage. To ameliorate such issues, high temperatures, pressures, and flow rates have been used, but to a limited effect [57, 58].

4.2.2 Segmented-Flow Microfluidics

Segmented-flow microfluidic systems solve the most significant problems associated with continuous-flow systems. In such systems, an additional immiscible phase (which can be a gas or liquid) is brought together with the reaction mixture in such a way that the reaction mixture spontaneously segments into a series of slugs (Figure 4.3c) or droplets (Figure 4.3d) surrounded by the continuous

carrier fluid. Intensive research in the general area of droplet-based microfluidics over the past decade has cemented the basic platform as an important (and perhaps the dominant) subset of microfluidic techniques [59]. Specific advances include developments in chip fabrication [60], an improved understanding of droplet dynamics [61], and the establishment of a variety of functional droplet components that can be integrated to generate complex workflows [62]. With respect to continuous-flow systems, droplet-based microfluidic reactors provide for enhanced analytical throughput, superior mass transport, dynamic manipulation of the reaction environment, and reliable automation [63].

Because droplets are generated in a controllable, rapid, and reproducible manner, NP synthesis within droplets almost always results in excellent reaction efficiencies and reduced polydispersity of particle populations. Furthermore, confinement of reagents within droplets prevents cross-contamination and enhances the efficiency of heat transfer and reagent mixing [64]. In general, droplet-based microfluidics opens up unprecedented opportunities for the synthesis of novel and bespoke NPs.

Within droplet-based microfluidic reactors, accurate handling and manipulation of droplets can be achieved using a wide range of functional components, such as droplet sorters, mergers, splitters, mixers, and traps [59, 65]. Such manipulations are basic elements within more complex and integrated workflows, allowing sophisticated multistep procedures to be carried out in an uninterrupted manner.

Controllable merging of droplets is a crucial technique that allows the initiation of reactions between droplets containing different precursors. This operation can be achieved by either passive or active means. As shown in Figure 4.4a, Niu et al. [66] reported a passive merging strategy, in which a droplet entering the chamber was slowed by a pillar array allowing a second droplet to catch it, whereupon the surface tension was overwhelmed by the hydraulic pressure and two droplets merged. Active droplet merging is most normally achieved via the application of electromagnetic forces, where charged droplets are brought together using electrostatic forces, and a high-frequency electric field is applied to destabilize the interface and induce merging [70].

Sorting is an essential manipulation technique when collecting or processing specific droplets within a segmented flow. Sorting enables the distribution and separation of droplets into different downstream locations. Again, sorting may be achieved by either passive or active techniques. In passive sorting, droplets are guided to different locations based on variations in droplet properties and channel geometries [71, 72]. A representative example of passive droplet sorting is the system reported by Tan et al. [73]. In this system, the microfluidic channels are designed so that the flow stream carrying the smaller droplets flows into a side channel, while the larger droplets flows through the main channel. Active sorting is realized through the application of electric fields [67], magnetic fields [74], or mechanical forces [75]. Figure 4.4b shows an example of active sorting using high-speed dielectrophoresis [67]. Here, generated droplets flow toward a Y-shaped junction containing two branching channels of different lengths. Because the hydraulic resistance is lower in the left branch, droplets will go through this route in the absence of an electrical field, but when an electrical

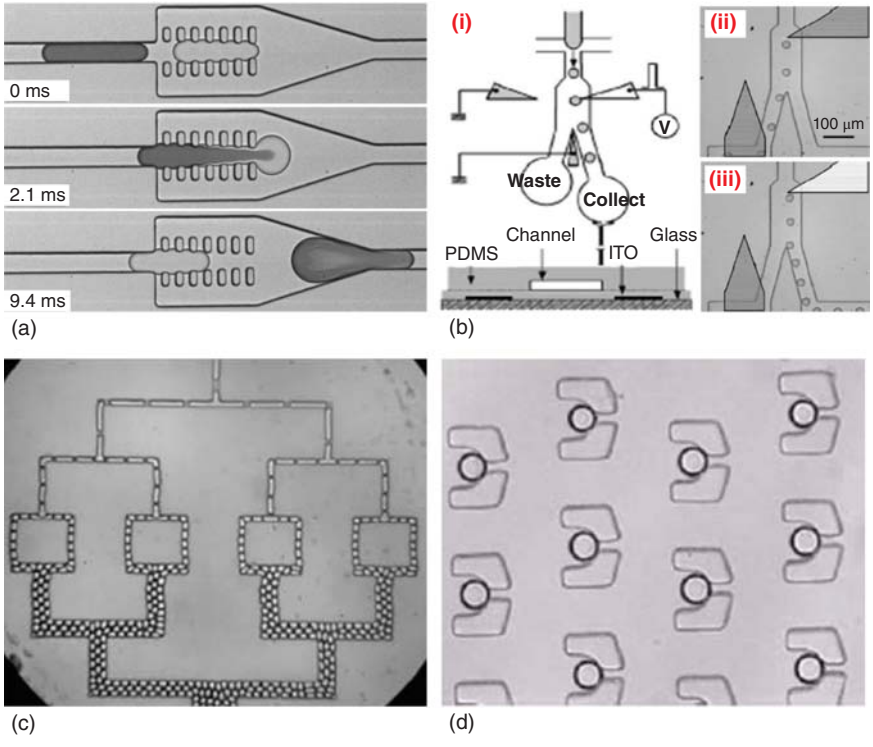

Figure 4.4 Droplet manipulations in microfluidics. (a) Droplet merging in an asymmetrical coalescence chamber. Source: Niu et al. 2008 [66]. Reproduced with permission of Royal Society of Chemistry. (b) Dielectrophoretic droplet sorting. Source: Ahn et al. 2006 [67]. Reproduced with permission of American Institute of Physics. (c) Sequential droplet splitting in a bifurcated network. Source: Link et al. 2004 [68]. Reproduced with permission of American Physical Society. (d) Droplet trapping in an array. Source: Huebner et al. 2009 [69]. Reproduced with permission of Royal Society of Chemistry.

field is applied, droplets are pulled into the right branch by a dielectrophoretic force.

Droplet splitting defines the process of dividing droplets into smaller ones. The most straightforward (passive) method involves geometry-mediated splitting, where a channel bifurcation is used to split a droplet into two daughter droplets (Figure 4.4c) [68]. Active splitting methods, involving the application of electric fields [76], heat [77], and radiation [78] have also been highly successful in allowing controlled droplet splitting.

Finally, droplet trapping allows the capture of large numbers of droplets within a specified area. As shown in Figure 4.4d, Huebner et al. [69] reported a method to trap droplets using a single-layer PDMS chip. The simple microfluidic array reported was able to trap and monitor hundreds of individual pl-volume droplets simultaneously. Droplets could be trapped, incubated, and retrieved at will and without the use of external stimuli. Considered together, such droplet manipulation methods ensure that droplet-based reaction platforms define a versatile

technology set and in the current context enable multistep processing and synthesis of QDs.

4.3 Continuous-Flow Microfluidic Synthesis of Quantum Dots

Initial investigations into the use of microfluidic systems for QD synthesis leveraged continuous-flow formats to overcome some of the inherent disadvantages of bulk synthesis methodologies. Since the first publication in 2002 [37], tremendous progress has been made in expanding the capabilities and applications of continuous-flow microfluidic reactors. In the following section, we present an overview of the key developments in the context of the materials and structures that have been explored, starting from simple homogenous core-type single-compound QDs through to complex multishell heterogenous systems.

4.3.1 Homogenous Core-Type Quantum Dots in Continuous Flow

4.3.1.1 Cadmium Sulfide (CdS)

QDs composed of a single compound, with no shells or gradients in their structure, represent the simplest materials class. It was through the synthesis of such materials that the pioneering bulk synthesis routes were established. However, these (now traditional) approaches suffer from an inability to control local reaction conditions, which only becomes worse as the reactions are scaled up, and almost always results in polydisperse product populations [79]. In a similar manner to bulk methods, pioneering microfluidic-based syntheses of QDs addressed core-type materials. The first report of QD synthesis within a microfluidic reactor was presented by Edel et al. at Imperial College London in 2002, with the demonstration of the controlled production of CdS NPs [37]. This work elegantly showcased the benefits of miniaturization in asserting tighter control over the physical conditions of the reaction, ensuring chemical homogeneity and temperature uniformity within the reaction volume to produce CdS QD populations with reduced polydispersity.

Although efficient thermal transfer is an inherent feature of microfluidic reactors, achieving chemical homogeneity within the reaction environment is nontrivial owing to the absence of turbulence in microengineered structures [80]. To overcome this problem, Edel et al. [37] implemented a continuous-flow reaction format based on the concept of parallel lamination (Figure 4.5a). This design splits both precursors (sodium sulfide and cadmium nitrate) into 16 multichannel streams, before bringing them into contact within a reverse network of partial flows. Because diffusion timescales are proportional to the square of the diffusion distance, such a multistream approach decreased the diffusion distance by a factor of 16 and reduced mixing times by a factor of 256. After nucleation and growth had proceeded, freshly synthesized QDs were fed into a quartz flow cell coupled to the chip outlet, allowing in-line (i.e. post QD formation) extraction of absorption spectra (Figure 4.5b). The results demonstrated two important

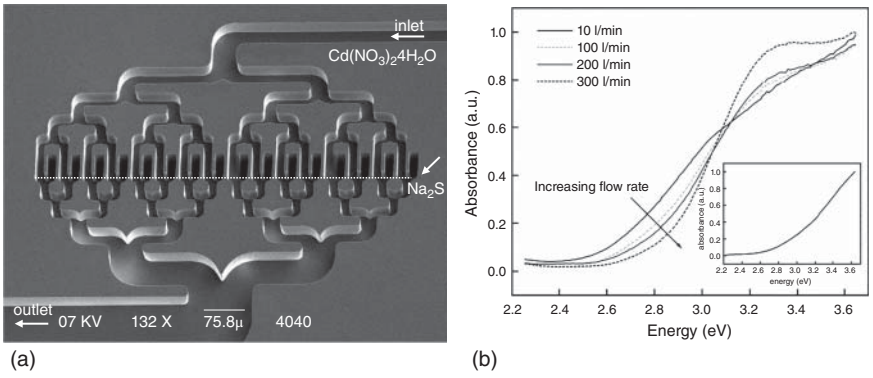

Figure 4.5 (a) Image of a microfluidic mixer based on the concept of parallel lamination. The two precursor inlets are split into 16 multichannel streams before being brought into contact at the dotted line. Only the top layer (for one precursor inlet) is visible. After mixing, the channels are recombined to form one outlet channel; (b) absorption spectra of synthesized CdS QDs as a function of volumetric flow rate. Inset: Absorption spectra of CdS QDs produced in a bulk reactor. Source: Edel et al. 2002 [37]. Reproduced with permission of Royal Society of Chemistry.

features. First, the slopes of all the absorption profiles from the microfluidic reactor were steeper than those obtained from a bulk reactor, demonstrating a reduction in NP polydispersity. Second, the slope of the absorbance profiles progressively increased as a function of volumetric flow rate, indicating a reduction in QD coalescence and a further decrease in particle polydispersity. Through this work, the authors elegantly demonstrated the distinct advantages of microfluidic synthesis over bulk methods, creating a new paradigm for the production of QDs.

4.3.1.2 Cadmium Selenide (CdSe)

CdSe-based NPs have been integral to the development of QDs and are the most studied and applied core material. The synthesis of CdSe core-type homogenous structure QDs in a microfluidic system was demonstrated by Marre et al. at the Massachusetts Institute of Technology in 2008 [58]. This work was notable for its use of supercritical fluids to overcome key limitations in the types of solvents that can be applied in microfluidics systems. In general terms, a given solvent must dissolve reaction precursors under ambient conditions and remain in the liquid phase over a wide temperature range. These requirements severely limit the number of solvents, and therefore, the variety of ligands and precursors, that are compatible with microfluidic reactors. A compounding problem in this respect is that many available solvents are of a high viscosity, resulting in slow mixing, extended residence-time distributions (RTDs), and broad nanocrystal size distributions (>10%). One approach to overcome such limitations is through the application of supercritical fluids [81, 82]. At high pressures, a solvent will eventually reach a supercritical regime, where the fluid solubilizes a wide range of compounds in a similar manner to a liquid, while displaying the high miscibility and fast diffusion rates typical of gases [83]. With these advantages, supercritical fluids offer new opportunities for the microfluidic synthesis of QDs. Marre et al.

used such solvents in the continuous-flow synthesis of CdSe QDs within a silicon/Pyrex microreactor that was able to withstand high pressures (Figure 4.2a) [58]. In this study, the entire setup was first pressurized using nitrogen gas. The precursor solutions were then delivered into the reactor and mixed at room temperature before entering a high-temperature reaction zone, where QD nucleation and growth was initiated. The reaction mixture ultimately exited the microreactor at a low temperature, quenching further QD growth, and was collected in a high-pressure reservoir. To provide a direct comparison for their studies, the authors synthesized CdSe QDs in both a conventional solvent (squalene) and a supercritical fluid (sc-hexane). They explored the influence of residence time, precursor concentration, and solvent phase on the QD size, nuclei concentration, and size distribution. Notably, and as shown in Figure 4.6b, results demonstrated that QD size varied as a function of residence time, leading to a red shift in the photoluminescence (PL) spectra. In comparison to squalene, the authors also observed that the use of sc-hexane led to a significant decrease in the QD size distribution, reported through a reduction in the full width at half-maximum (FWHM) of the emission peak (Figure 4.6b). The two main contributing factors to this decrease in size distribution are the RTD difference of the solvents and the kinetics of nanocrystal formation. Specifically, hexane has a 10–20-fold lower viscosity compared with squalene, leading to a much lower RTD. Accordingly, the reaction mixture in sc-hexane experiences more uniform reaction conditions. Furthermore, sc-hexane possesses a higher supersaturation point, which induces a higher initial concentration of nuclei for subsequent growth, fast depletion of precursors in solution, and a short nucleation phase.

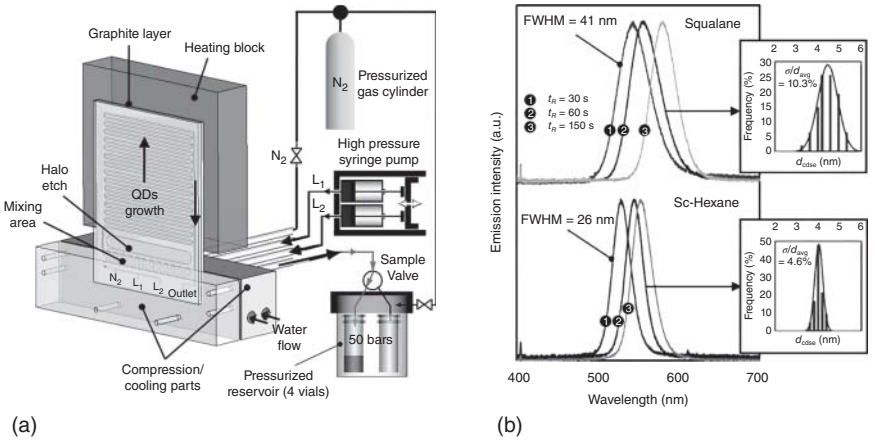

Figure 4.6 (a) Schematic of experimental setup used for supercritical fluid-assisted synthesis of QDs. The high-pressure microreactor is integrated with compression-cooling parts, a high-pressure syringe pump, a high-pressure valve, and a high-pressure reservoir containing four vials; (b) PL spectra at varying residence times (t_R) and QD size distributions. Size distributions were determined for samples run at $t_R = 60$ seconds. Source: Marre et al. 2008 [58]. Reproduced with permission of John Wiley & Sons.

4.3.2 Heterogenous Core/Shell Quantum Dots in Continuous Flow

Core-type homogenous structure QDs perform well in idealized conditions; however, in practice, they suffer from some innate problems. The size and shape of QDs make their surfaces highly energetic and reactive. Such a reactive state can be somewhat passivated by the presence of surface capping ligands. Nevertheless, in practice, it is extremely difficult to arrest surface reactions such as oxidation. When these reactions occur, energetic traps are created where electrons of the all-important exciton become ensnared, thus prohibiting PL. In the bulk synthesis of QDs, a range of strategies to cap QD cores through epitaxial growth of an inorganic shell have proved successful. Such a shell has a band gap offset versus the core, rendering it energetically unfavorable for the electrons or holes of the excitons to diffuse into the shell. This general approach has become a standard solution to the problem of fluorescence quenching of QD cores. Thus, it is imperative that microfluidic approaches are capable of multistep growth to create heterogenous, or core/shell, QDs. Fortunately, this challenge was met by a series of innovations, on a variety of QD material types, as described now.

4.3.2.1 Zinc Selenide/Zinc Sulfide (ZnSe/ZnS)

In 2012, Kwon et al. at the Korea Advanced Institute of Science and Technology [84] reported a novel approach for the microfluidic synthesis of ZnSe/ZnS QDs. This work is notable for its demonstration of the continuous synthesis of core/shell-type QDs via a single injection of precursors, thus avoiding the need for more complex multistep synthetic routes [85, 86]. Briefly, the authors fabricated a cyclic olefin copolymer (COC) microfluidic reactor via injection molding [87]. Importantly, COC is stable under acidic and basic conditions and resistant to many organic solvents, while also being transparent in the visible region of the electromagnetic spectrum [88]. The developed microreactor consisted of three sections, one for precursor mixing, one for ZnSe core formation, and one for ZnS shell coating (Figure 4.7a). The precursors (Zn, Se, and S) were introduced together, with Zn and S being consumed first to produce ZnSe cores, followed by a reaction between the Zn and S precursors to form the ZnS shells. The resulting UV/vis absorption and PL spectra of the ZnSe/ZnS QDs are shown in Figure 4.7b,c. Significantly, it was observed that ZnSe/ZnS QDs exhibited significantly stronger emission than the ZnSe QDs. After the optimization of flow rates, the emission intensities increased by 270% (compound **12** in Figure 4.7), with a narrower size distribution implied by a reduced FWHM of the band edge emission. Accordingly, through the use of thermoplastic microreactors, the authors opened a new and facile route for the microfluidic synthesis of core/shell QDs.

4.3.2.2 Cadmium Selenide/Zinc Sulfide (CdSe/ZnS) and Cadmium Telluride/Zinc Sulfide (CdTe/ZnS)

As noted, QDs have attracted much interest as tools in biological sensing [89]. For such applications, it is necessary to put the final QD constructs into aqueous media and ensure maintenance of their advantageous colloidal and optical properties. This is typically achieved through the addition of a layer of organic ligands bearing hydrophilic groups and QD-binding moieties. QD synthesis can

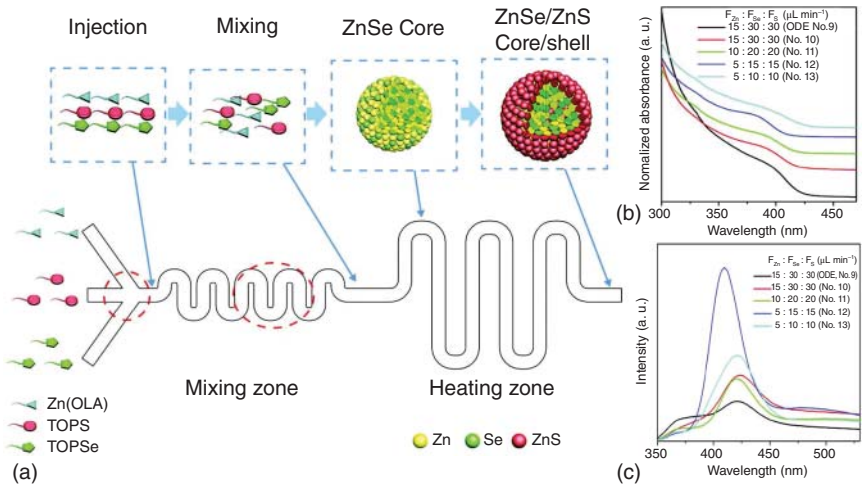

Figure 4.7 (a) A schematic of ZnSe/ZnS QD synthesis in a thermoplastic microfluidic reactor; (b) UV/vis absorption spectra; and (c) PL spectra of synthesized QDs as a function of precursor flow rate. Sample No. 9 is composed of ZnSe QDs, while samples No. 10, 11, 12, and 13 are ZnSe/ZnS QDs. Source: Kwon et al. 2012 [84]. Reproduced with permission of John Wiley & Sons.

be performed in aqueous conditions; however, it is much more common to carry out the synthesis in organic solvents and then perform a post-processing step to transfer them into aqueous solution. Accordingly, such a process of QD core synthesis, followed by inorganic shell growth and hydrophilic ligand attachment, makes for relatively complex synthetic procedures.

In 2010, Kikkeri et al. at the Max Planck Institute for Colloids and Interfaces [90] reported the synthesis of biofunctionalized core/shell QDs in microfluidic reactors. The researchers used a series of glass microfluidic reactors to synthesize and functionalize CdSe/ZnS and CdTe/ZnS core/shell QDs bearing carboxyl groups and carbohydrates. The synthesis of the QD cores, growth of the inorganic shells, and functionalization were performed in discrete stages using separate continuous-flow microfluidic chips (Figure 4.8a), with purification being performed off-chip after each step. Briefly, the Cd and Se or Te precursors were injected into a first device to form the QD cores. The QDs were then purified off-chip and injected into a second device with a ZnS precursor to grow the shell layer. The core/shell QDs were purified off-chip again and finally injected into a third device for ligand exchange and surface modification before being precipitated and taken into aqueous solution. Significantly, the authors were able to demonstrate the synthesis of CdSe and CdTe QDs of controllable size by adjusting the reaction time within the first microfluidic device (Figure 4.8b), noting that longer reaction times resulted in a larger PL FWHM and decreased PL quantum yield (QY). However, upon formation of the ZnS shell in the second device, the PL QY increased from 23% to 31% because of the stabilizing effect of the shell. Successful functionalization with carboxyl groups and carbohydrates in the third microfluidic device was confirmed by

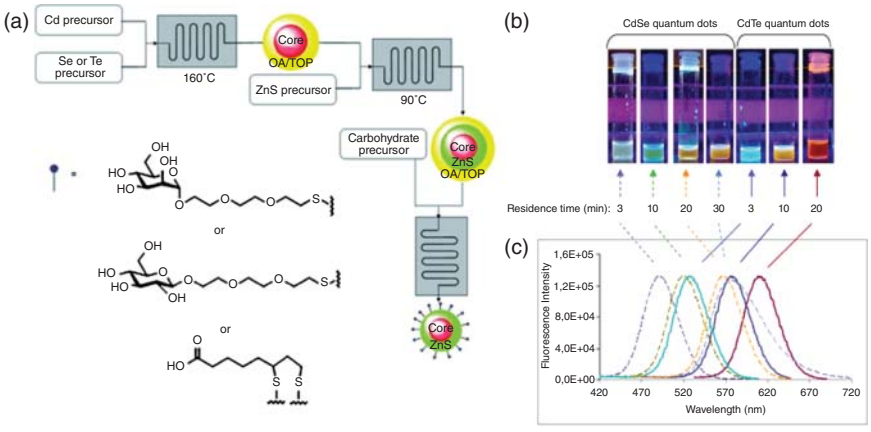

Figure 4.8 (a) Schematic of a microreactor setup for the synthesis of carboxylated or carbohydrate-coated CdTe/ZnS and CdSe/ZnS core/shell QDs. Three continuous-flow microfluidic chips were used for each step: (1) synthesis of the QD core, (2) formation of shell layer, and (3) functionalization with the biologically relevant molecule. (b) Images of CdSe and CdTe QDs under UV light and (c) normalized photoluminescence spectra of CdSe (---) and CdTe (—) QDs as a function of reaction residence time. Source: Kikkeri et al. 2010 [90]. Reproduced with permission of John Wiley & Sons.

studying the interactions between the sugar-coated QDs and lectin concanavalin A (ConA). Some QDs were functionalized with α-mannose, while others were functionalized with β-galactose. Because ConA binds with α-mannose and not β-galactose, addition of ConA to α-mannose-coated QDs caused the QDs to aggregate, whereas ConA had no effect on the β-galactose-coated QDs. This was verified via turbidity measurements, with the addition of ConA to α-mannose-coated QDs resulting in immediate turbidity, whereas little turbidity was observed with β-galactose-coated QDs. Overall, this work was notable for its synthesis of biologically applicable core/shell QDs, a feat that is relatively challenging even on a bulk scale.

4.3.2.3 Copper Indium Sulfide/Zinc Sulfide ($CuInS_2$/ZnS)

The presence of Cd in traditional QD formulations, and its associated toxicity, has led to efforts to find alternative formulations that use minimally toxic elements but still possess the advantageous properties of traditional QDs. Recently, copper indium sulfide ($CuInS_2$) QDs have emerged as an interesting competitor in this field. They are heavy metal-free and can emit at wavelengths between the visible and NIR regions of the electromagnetic spectrum [91, 92]. The initial exploration of $CuInS_2$ QD synthesis routes utilized bulk methods to good effect, but obvious inherent issues regarding varying local reaction conditions across bulk solutions remained.

In 2016, Tian et al. from Bayer Technology Services [93] used a continuous-flow microfluidic approach for the facile and large-scale synthesis of $CuInS_2$ and $CuInS_2$/ZnS QDs. This required reformulation of the bulk precursor solutions to ensure compatibility with microfluidic processes and involved replacing copper actinium (CuAc) with copper(I) iodide (CuI) because of its superior

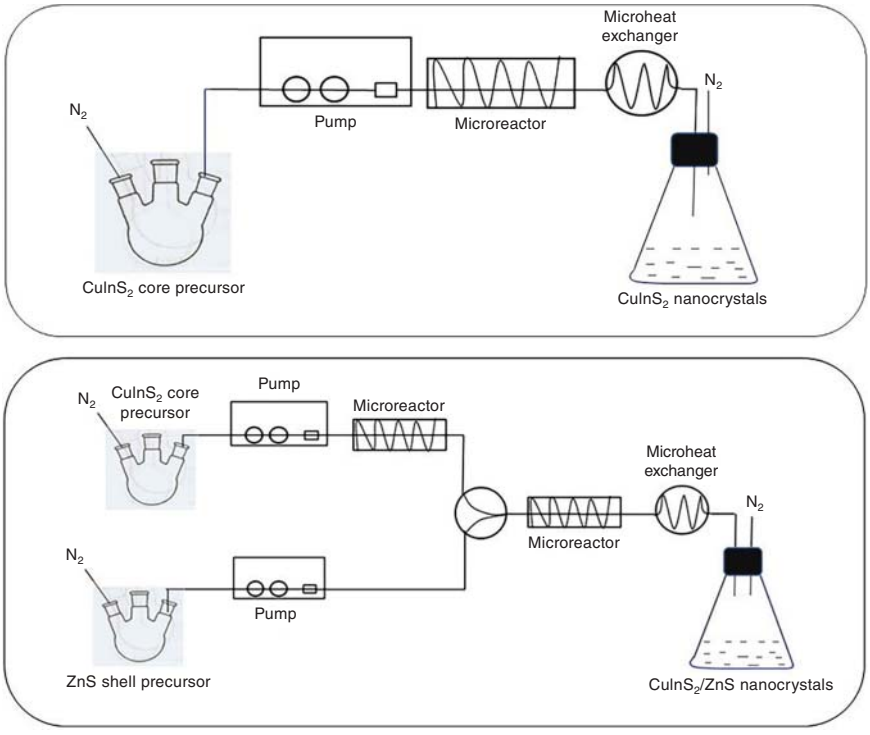

Figure 4.9 A simplified schematic of a $CuInS_2$ core QD (top) and $CuInS_2$/ZnS core/shell QD (bottom) continuous-flow synthesis. Source: Tian et al. 2016 [93]. Reproduced with permission of Elsevier.

stability under ambient conditions. They synthesized core-type or core/shell QDs in microreactors that fed directly into a microheat exchanger to rapidly cool the reactions and halt particle growth, yielding populations of stable QDs (Figure 4.9).

For the synthesis of core-type $CuInS_2$ QDs, the authors used a single microreactor and discovered that lower flow rates led to higher PL QYs. Indeed, they reported an optimized value of 28%, which was the highest ever value obtained for $CuInS_2$ QDs. The products exhibited a narrow-size distribution, and the workflow achieved a synthesis rate more than twice that of previous reports. For ZnS shell formation, the authors incorporated a second microreactor, with core and shell growth occurring serially before the reaction solution was fed into the heat exchanger. Interestingly, the authors implemented staged temperature variations and a distributed feed to ensure slow and homogenous shell formation. Motivated by multistep bulk synthesis procedures, the staged temperature approach incorporated three microreactors at different temperatures, with core growth at 250 °C and shell growth at 180 and 230 °C. This resulted in a reduction in crystal defects in the ZnS shell and led to $CuInS_2$/ZnS QDs with a 49% PL QY. In the distributed feed approach, the shell precursor was injected four times, instead of just once, to maintain a high concentration of precursor during shell formation.

The authors found that each additional injection of shell precursor led to an increase in PL QY. With the first demonstration of a fully continuous system for $CuInS_2$ and $CuInS_2$/ZnS QD synthesis, this general approach is a promising step toward large-scale high-quality production of a promising class of Cd-free QDs.

4.3.2.4 Indium Phosphide/Zinc Sulfide (InP/ZnS)

As previously described, the production of microreactor systems that incorporate consecutive reaction steps is important in facilitating the transfer of bulk approaches to the microscale. In this vein, Baek et al. at the Massachusetts Institute of Technology [94] developed a multistage synthesis platform incorporating up to six high-temperature and high-pressure microchip reactors (Figure 4.10a). The system was used to synthesize InP/ZnS core/shell QDs with narrow-size distributions, tunable emission peaks, and high PL QYs. To enhance the versatility of the platform, the authors used silicon-Pyrex chips to enable high-temperature and high-pressure reactions, with octane being used as a solvent, because of its low dispersion for both core and core/shell growth at or near supercritical conditions. InP cores were synthesized within the first two microreactors, while nanocrystal growth was initiated in the third. The ZnS shell was formed in the following three microreactors, where 10 subchannels maintained a low concentration of the shell materials and prevented undesired ZnS nucleation (Figure 4.10b). A customized in-line optical device was used to characterize the absorption and emission of the synthesized QDs.

By adjusting the number of precursor injections within the first two microreactors, InP QD size could be precisely controlled. Furthermore, the addition of myristic acid allowed the platform to overcome traditional limitations in the growth of large InP QDs (Figure 4.10e). The PL FWHMs were as low as 42 nm, while the PL QYs were as high as 40%. Importantly, the authors confirmed that their InP/ZnS QDs remained luminescent after phase transfer into aqueous solution. To demonstrate the versatility of the platform, InP/ZnS QDs were also synthesized using low boiling point short-chain alkyl thiols as solvents. Interestingly, the authors were able to adjust the temperature and injection sequence of their modular platform to synthesize InP/ZnSe, InP/CdS, and InAs/InP QDs.

4.3.3 Heterogenous Core/Multishell Quantum Dots in Continuous Flow

When adding shell layers to QD cores, there are two major factors that must be considered. First, the lattice mismatch between the core and the shell should be minimized to allow the synthesis of QDs with minimal lattice defects. Second, the QD shell should have a band gap significantly higher than the core to prevent electrons tunneling from core to shell. Although heterogenous core/shell QDs demonstrate superior PL efficiencies compared to homogenous core-type QDs, it is uncommon for a single shell material to fulfill both criteria. To tackle this, researchers have produced core/multishell QDs, where epitaxial growth of multiple shells are sequentially performed, which provides an intermediate layer to transition between the lattice mismatches of the core and outermost shell

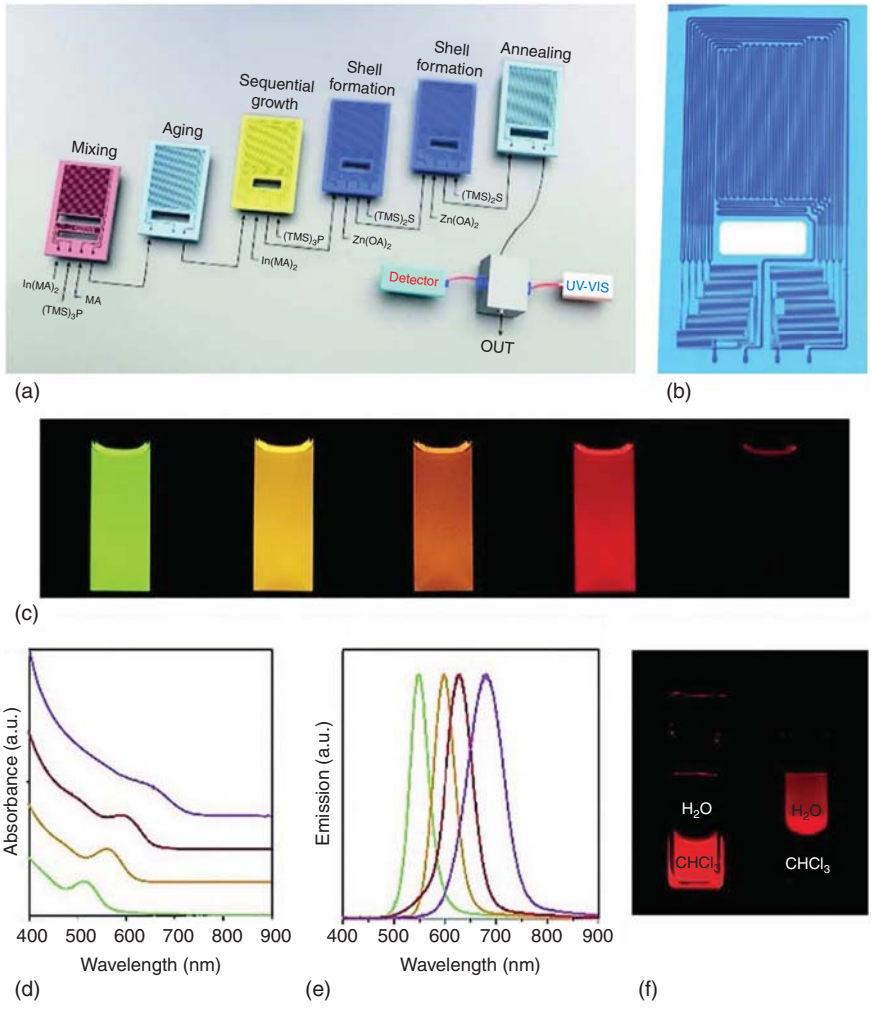

Figure 4.10 (a) A multistage microfluidic platform for the synthesis of InP/ZnS core/shell QDs. The first three stages are used to synthesize InP cores, while the last three are used to synthesize the ZnS shell layer; (b) a shell formation microreactor consisting of 10 subchannels; (c) InP/ZnS QDs of various sizes under 365 nm illumination; (d) absorption and (e) emission spectra of the InP/ZnS QDs; and (f) phase transfer of the InP/ZnS QDs from chloroform (left) to water (right). Source: Baek et al. 2018 [94]. Reproduced with permission of John Wiley & Sons.

while maintaining their large band offset. These heterogenous core/multishell structures have become established as an important class of QD; therefore, it is critical that microfluidic reactors are able to produce QDs with multiple shells engineered in a precisely defined manner.

4.3.3.1 Cadmium Selenide/Cadmium Sulfide/Zinc Sulfide (CdSe/CdS/ZnS)

In contrast to systems that incorporate increasing numbers of processing units to mimic the complexity associated with bulk synthetic methods, other

studies have focused on reformulating reaction precursors to naturally favor the formation of specific QD structures. This approach is particularly attractive when the reaction products are complex, for example, when core/multishell structures are desired. A prominent example in this respect is CdSe/CdS/ZnS. Although ZnS shell formation is known to significantly stabilize CdSe QD cores, the extent of the improvement is inherently limited by the relatively large lattice mismatch between ZnS and CdSe [95], which creates lattice strains at the interface between the core and shell [96]. Through the introduction of a CdS intermediate layer, studies have demonstrated a reduction in lattice strain and a corresponding increase in PL QY using bulk reactors [96]. Because of the inherent complexity of such a structure, however, some innovation is required to transfer the synthesis to the microscale.

In 2015, Naughton et al. from the University of Illinois at Urbana-Champaign developed a continuous-flow platform for the synthesis of CdSe/CdS/ZnS QDs [97]. Interestingly, the focus of this work was on the formulation of the Cd, Se, S, and Zn precursors, with a relatively simple continuous-flow setup being used (Figure 4.11). Precursor mixing could be done before injection, obviating the need for online mixers and simplifying microreactor design. The authors explored various core/shell compositions and compound alloys. For the synthesis of CdSe/CdS/ZnS QDs, the Cd precursor was cadmium oxide (CdO) in oleic acid, the Se precursor was trioctylphosphine selenide (TOP-Se) in octadecene (ODE), and the S precursor was trioctylphosphine sulfide (TOP-S) in ODE. Zn for the shell synthesis was supplied from zinc diethyldithiocarbamate (Zn $DDTC_2$) in TOP, which thermally decomposes into ZnS. After mixing the precursors and injecting them into the flow reactor, the CdSe cores formed first, followed by the CdS intermediate layers, and finally the ZnS shells. This occurred since Se has a higher reactivity than S. ZnS was then formed over the CdSe/CdS NPs through Zn $DDTC_2$ decomposition.

The authors elegantly showed that they could tune the emission wavelength of the CdSe/CdS/ZnS QDs by adjusting the average residence time and the number of ZnS layers. By doing this, they were able to obtain emission wavelengths

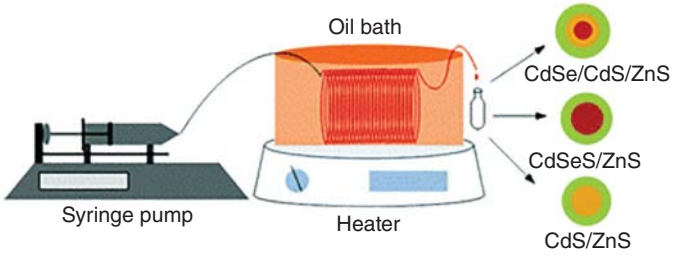

Figure 4.11 A schematic illustrating the continuous-flow setup used to synthesize heterogenous core–multishell QDs. The syringe pump is used to motivate reagents, while an oil bath maintains the temperature of the reactor. The synthesis of CdSe/CdS/ZnS, CdSeS/ZnS, and CdS/ZnS QDs was demonstrated. Source: Naughton et al. 2015 [97]. Reproduced with permission of Royal Society of Chemistry.

covering the entire visible region of the electromagnetic spectrum. Additionally, screening studies indicated that two ZnS layers led to the highest quality QDs, agreeing with literature reports [96]. Optimized CdSe/CdS/ZnS QDs had a 60% PL QY, which is significantly above the 12% for CdSe/ZnS core/shell QDs synthesized using the same platform.

4.3.4 Summary of QD Classes

In this section, we have introduced continuous-flow microfluidic synthesis of a wide range of QDs, including homogenous core-type, heterogenous core–shell, and heterogenous core/multishell QDs. Homogenous core-type QDs are the most classic structures and contain only a single compound. However, they are vulnerable to surface degradation and oxidation because of insufficient protection from their organic capping ligands. Therefore, they are commonly capped with a second semiconductor compound – epitaxially grown upon the core – to completely passivate the surface and provide a band gap offset to restrict electrons from tunneling into the shell. However, it is often advantageous to grow multiple shells of different compounds, which allows better tuning of the lattice mismatch and band gap offset. These are termed core/multishell QDs.

4.4 Segmented-Flow Microfluidic Synthesis of Quantum Dots

As discussed, continuous-flow reactors provide significant advantages over bulk synthesis methods. However, there are two common problems that ultimately limit their efficiency and application. First, in all continuous-flow microfluidic devices, viscous drag at the channel walls causes nonuniform fluid velocities across the width of the channel, leading to finite and appreciable RTDs and ultimately a broadening of achievable particle size distributions [51, 57]. This problem is especially acute in high-viscosity solvents, which are commonly employed in QD synthesis. Second, deposition of solid material on channel walls over time is almost unavoidable. This severe issue constrains reactor lifetimes, which in turn limits possibilities for reaction scale-out.

An effective method to overcome both the above problems is to employ a segmented flow rather than a continuous flow. Droplet microfluidic systems not only minimize dispersive flow and solid deposition but also confer rapid mass and heat transfer, high-throughput operation, precise reagent control, and reliable automation. We now discuss some key droplet-based microfluidic strategies for the synthesis of QDs, with a focus on the QD materials and structures that have been explored. Additionally, examples of kinetic studies of QD nucleation and growth, multistep synthesis techniques for multicomponent QD synthesis, and *in situ* spectroscopic modules for QD characterization during (online) and after (in-line) particle formation are described.

4.4.1 Homogenous Structure Quantum Dots in Segmented Flow

4.4.1.1 Cadmium Sulfide (CdS)

Reports on the synthesis of QDs in segmented flows started appearing in the literature shortly after the initial continuous-flow studies, with Shestopalov et al. at the University of Chicago initially reporting the synthesis of QDs in droplet-based microfluidic reactors in 2004 [98]. In this work, the authors described an aqueous synthesis of CdS QDs at room temperature within a PDMS reactor. They performed elegant control experiments to demonstrate the efficacy of their system, including a direct comparison between continuous flow and segmented flow in the same device (Figure 4.12). For the continuous-flow experiments, streams of the Cd ($CdCl_2$, cadmium chloride) and S (Na_2S, sodium sulfide) precursors were brought together, but separated by a stream of buffer, and injected into a water stream at a T-junction (Figure 4.12A). Using such an approach, solid deposition onto channel surfaces began almost immediately, rendering the device ineffective after a few tens of minutes. In contrast, when the water stream was replaced with an oil stream, the aqueous reaction solution spontaneously segmented into droplets because of the shear force from the fluorinated carrier oil (Figure 4.12B), with subsequent synthesis of CdS QDs occurring only inside the droplets. In

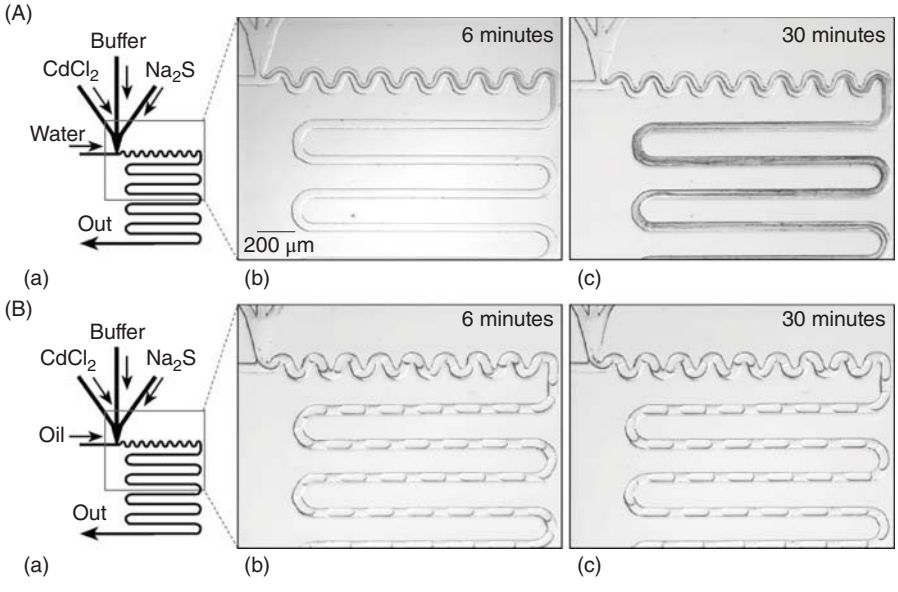

Figure 4.12 A droplet-based microfluidic reactor for CdS QD synthesis developed by Shestopalov et al. prevents fouling of microchannels during QD synthesis. (A) (a) A schematic showing the continuous-flow microreactor. (b, c) Images demonstrating the accumulation of solid CdS on the channel walls after 6 and 30 minutes of continuous flow operation; (B) (a) A schematic of the segmented-flow microreactor. (b, c) Images demonstrating the lack of solid deposition after 6 and 30 minutes of droplet flow. Source: Shestopalov et al. 2004 [98]. Reproduced with permission of Royal Society of Chemistry.

comparison, after 30 minutes of operation, there was no observable deposition of solid on the channel walls. That said, the scope of aqueous syntheses of QDs is somewhat limited, and thus, it is important for segmented-flow microfluidic systems to adapt to the more common organic solvents.

4.4.1.2 Cadmium Selenide (CdSe)

Reactions in long-chain, high-viscosity solvents typically require high temperatures to trigger the nucleation and growth of QDs. This provides significant motivation to produce segmented-flow microfluidic reactor systems that can process organic solvents in a robust manner and operate at high temperatures.

One of the first droplet-based microfluidic reactors for high-temperature QD synthesis was reported by Yen et al. from the Massachusetts Institute of Technology [99], who used a gas–liquid segmented-flow microreactor to synthesize CdSe QDs at 260 °C. The reactor was fabricated in silicon and glass and incorporated multiple temperature-controlled zones (Figure 4.13). A heated aluminum block was used to define the high-temperature reaction zone, while water-chilled aluminum blocks were used for the inlet and quenching zones. The Cd and Se precursors were prepared by solubilizing cadmium 2,4-pentanedionate and selenium in squalene with long-chain ligands. By tuning the injection rates of the Cd and Se precursors, the authors attained good control of CdSe QD size, with significantly narrower size distributions and shorter reaction times

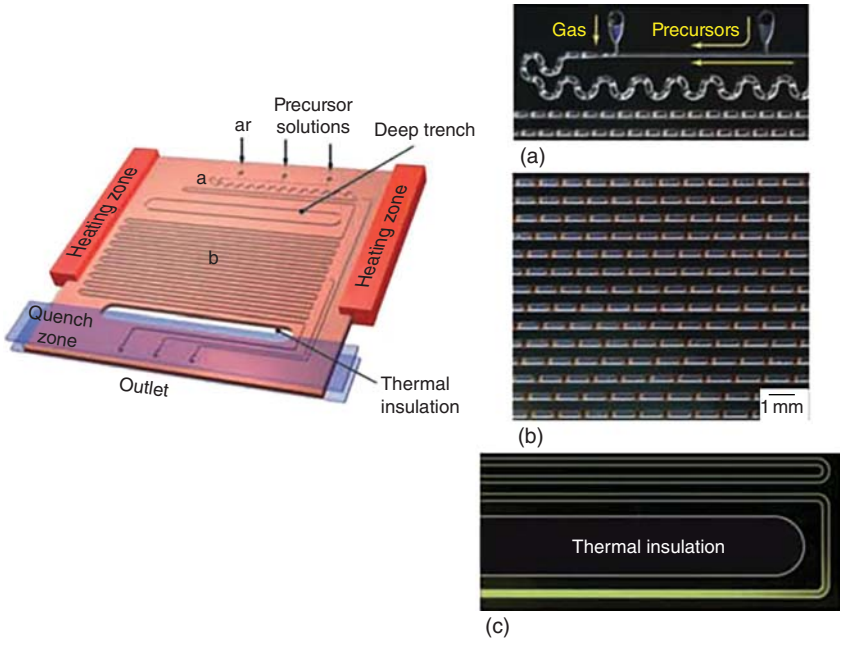

Figure 4.13 A gas–liquid slug microreactor with thermal control for CdSe QD synthesis. (a) Inlets for the precursors and gas before slug formation. (b) Reaction heating zone. (c) Time exposure image of the quenching region and outlet under UV radiation. Source: Yen et al. 2005 [99]. Reproduced with permission of John Wiley & Sons.

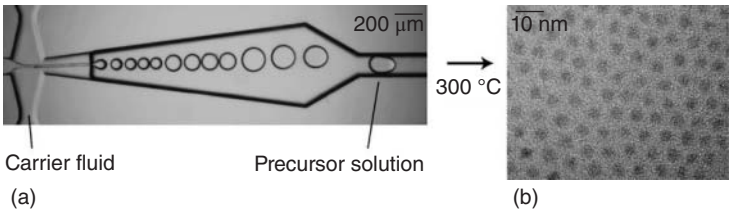

Figure 4.14 CdSe QD synthesis at temperatures between 270 and 300 °C in a liquid–liquid segmented microreactor with thermal control. (a) Droplets are generated by a cross-shaped nanojet injector. (b) Transmission electron micrographs of CdSe QDs synthesized in droplets of ODE within a PFPE carrier fluid at 300 °C. Source: Chan et al. 2005 [100]. Reproduced with permission of American Chemical Society.

compared to continuous-flow microreactors. Moreover, the PL FWHMs of CdSe QDs from their two-phase segmented-flow reactor ($\Delta\lambda = 30 \pm 2$ nm) were significantly narrower than those obtained in continuous-flow synthesis schemes ($\Delta\lambda = 34 \pm 5$ nm), which was attributed to the nondispersive motion of the reagent droplets [51].

Despite the promise shown by gas-liquid segmented-flow microfluidic platforms, there are two important limitations. First, the carrier gas severely limits the operating stability because its volume can be heavily affected by small changes in temperature or pressure. Second, solid products may still deposit onto the channel walls as the walls come into direct contact with the reaction solution. To address these issues, Chan et al. at the University of California, Berkeley [100], developed a high-temperature liquid–liquid segmented-flow microreactor for CdSe QD synthesis (Figure 4.14). Here, ODE was used as the discrete phase and a high-boiling point perfluorinated polyether (PFPE) oil as the continuous phase. To make droplets of ODE in PFPE over a wide range of flow rates, the authors fabricated glass microreactors with a cross-shaped nanojet injector (Figure 4.14a). PFPE was injected through the side arms of the cross while the ODE solution was injected from the top. The generated droplets then traveled through the 2.4 mm-long nozzle into a heating region where the reaction was initiated. This method allowed their microfluidic devices to maintain reproducible droplet flow. The QD synthesis proceeded by reacting cadmium oleate with a solution of TOP-Se/TOP at temperatures up to 300 °C, with successful product formation confirmed by TEM (Figure 4.14b). The liquid–liquid segmented flow completely eliminated solid deposition on the channel walls during the lifetime of the device (~5 hours), whereas analogous experiments under continuous flow showed clear deposition after only 20 minutes.

4.4.1.3 Lead Sulfide (PbS) and Lead Selenide (PbSe)

While Cd-based QDs have been shown to emit over the entire visible spectrum, their reach into the infrared spectrum is limited. Pb-based QDs are, in contrast, tunable across a broad region of the infrared (800–3000 nm) [101] and are attractive materials in various applications, such as solar cells, photodetectors, NIR lasers, and biological imaging [102–105]. In 2014, Lignos et al. at the Swiss Federal Institute of Technology in Zürich (ETH Zürich) [106] reported a segmented-flow

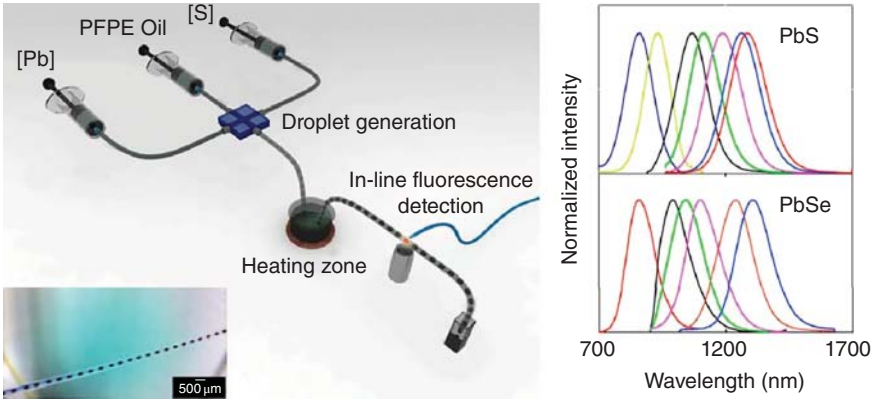

Figure 4.15 PbS QDs synthesis in a droplet-based capillary reactor with rapid in-line PL detection. (a) A schematic of the capillary microfluidic reactor, integrating an in-line NIR fluorescence detector; (b) tuning of the PL emission by variation of temperature for PbS and PbSe QDs. Source: Lignos et al. 2014 [106]. Reproduced with permission of American Chemical Society.

microfluidic system for PbS and PbSe QD synthesis using capillary tubing rather than the common chip formats discussed previously. Capillary reactors are typically easier to build, operate, and modify because of their modular construction using readily available components, while offering the ability of reaction scale-up [50].

In this work, the authors specifically used polytetrafluoroethylene (PTFE) tubing to define the microfluidic system (Figure 4.15a). Separate syringes loaded with the Pb precursor (lead oleate), S precursor (bis-(trimethylsily) sulfide), and the oil phase were used to deliver fluid into a polyether ether ketone (PEEK) cross, which served as a droplet generator. Formed droplets then traveled through the tubing to a heating zone, where the reaction proceeded at temperatures ranging between 80 and 155 °C. Droplets containing synthesized PbS QDs were then cooled to room temperature and monitored using an in-line fluorescence detection system. Such PbS QDs exhibited narrow-size distributions (5–7%) and improved PL QYs (~28%) versus comparable bulk-synthesized materials (~12%). In-line monitoring of the PL of individual droplets allowed ready optimization of reaction parameters and thus excellent control over QD PL (765–1580 nm for PbS and 860–1600 nm for PbSe), as shown in Figure 4.15b. Furthermore, synthesis reactions could be performed using their microfluidic setup for periods between three and six hours. Accordingly, such a system can be tuned to produce kilogram quantities of QDs per day.

4.4.1.4 Perovskite QDs

Lead halide perovskite QDs have attracted tremendous research interest in the past five years because of their remarkable photophysical and photovoltaic properties [107–109]. Similar to standard QDs, their PL properties can be controlled through variations in size and/or composition [110]. For the chemist, this means

that a rich and complex reaction parameter space must be accessed and explored to allow the synthesis bespoke materials with desirable properties. In this respect, segmented-flow microfluidic systems have been shown to be extremely effective tools, with a series of studies demonstrating fast parametric space mapping [111], shape evolution [112], and crystal growth mechanisms [113].

In a pioneering study, Kovalenko and coworkers at ETH Zürich [111] used a capillary-based microfluidic platform to synthesize $CsPbX_3$ (caesium lead halide) perovskite QDs. A key feature of the reaction platform was the integration of online detectors for monitoring both absorbance and fluorescence during QD nucleation and growth (Figure 4.16). Different lead halide precursors (denoted as PbX_2 and PbY_2) were premixed using a T-junction with a variable molar ratio of X to Y, denoted as R_2. The $PbX_\alpha Y_{(2-\alpha)}$ mixture was then delivered into a cross-mixer, where the Cs precursor (Cs oleate) was injected at a chosen ratio to Pb, denoted as R_1 (Figure 4.16a). In this way, R_1 and R_2 could be tuned separately and continuously, generating droplets containing varying precursor ratios. The droplets were subsequently motivated in a coil around a heating rod (Figure 4.16b), with the residence time being controlled by the total flow rate. Using this setup, the authors were able to synthesize $CsPbX_3$ QDs with real-time and continuous control of composition and PL (Figure 4.16b,c). Furthermore, ultrafast kinetic measurements (between 100 ms and 5 seconds after reaction initiation) and rapid parametric optimization experiments were performed. This study is not only an important demonstration of a new class of QDs synthesized within segmented

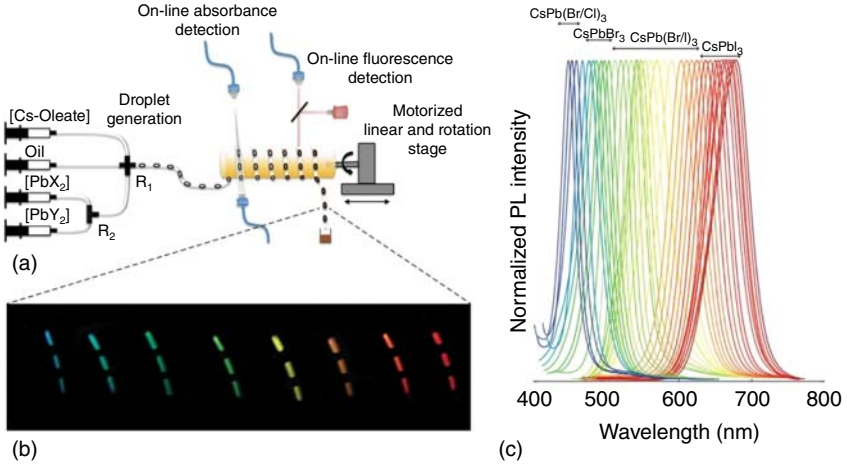

Figure 4.16 $CsPbX_3$ perovskite QD synthesis in a droplet-based capillary reactor with integrated online absorbance and fluorescence detection. (a) A schematic of the droplet-based microfluidic platform. The Pb/Cs ratio (R_1) and halide ratio (R_2) are continuously varied to allow precise tuning of the chemical contents within the droplets. The online absorbance and fluorescence detection systems are used to probe the product at a range of reaction times, and as early as 0.1 second; (b) an image of generated droplets using different precursor ratios. The picture was taken of the coiled heating zone under UV excitation (405 nm); (c) the whole visible spectrum can be covered by $CsPbX_3$ QD emission, as determined by online fluorescence measurements. Source: Lignos et al. 2016 [111]. Reproduced with permission of American Chemical Society.

flows but also a validation of such systems for exploring the reaction parameter space and performing rapid optimization.

4.4.2 Heterogenous Core/Shell Quantum Dots in Segmented Flow

4.4.2.1 Copper Indium Sulfide/Zinc Sulfide ($CuInS_2$/ZnS)

Although there have been many reports of homogenous core-type QD synthesis in segmented flow, examples of the synthesis of core/shell QDs via this approach are relatively rare. This is most likely because precise downstream dosing of droplets is challenging, which restricts somewhat the possibilities for multistage synthesis [114]. Nevertheless, Yashina et al. at ETH Zürich recently demonstrated the synthesis of $CuInS_2$/ZnS QDs in a two-stage droplet microfluidic platform that could independently and precisely dose droplets (Figure 4.17) [115]. Specifically, CuI (copper iodide) and $In(OAc)_3$ (indium triacetate) were used as metal precursors, 1-dodecanethiol as the sulfur source, and PFPE as the carrier fluid. All precursors and carrier fluids were loaded into glass syringes connected with PTFE capillaries. These solutions were then mixed, injected into the setup, and segmented into droplets at a PEEK cross unit. The resultant droplets of the reaction mixture were transferred to a copper-heating rod (with the reaction tubing coiling around), where the reaction was initiated and $CuInS_2$ QDs formed. After the first stage, $Zn(OAc)_2$ (zinc diacetate) precursor was injected into the flow from a side channel. The reformed droplets were then transferred to a second heating rod for growth of the ZnS shell. To monitor the optical properties of the synthesized QDs and to optimize the reaction parameters, two in-line PL detectors were used. This two-stage microfluidic

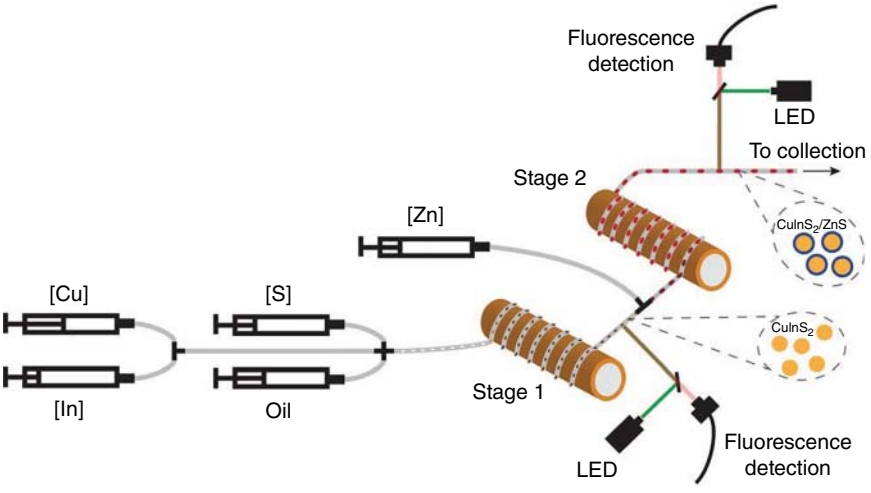

Figure 4.17 Core/shell $CuInS_2$/ZnS QDs synthesized in a two-stage droplet-based microfluidic platform. The first stage is used to synthesize the $CuInS_2$ core, and the second stage is used for growing the ZnS shell. Fluorescence detectors were used to monitor the products from the first stage ($CuInS_2$ core) and second stage ($CuInS_2$/ZnS core/shell QD). Source: Yashina et al. 2016 [115]. Reproduced with permission of Royal Society of Chemistry.

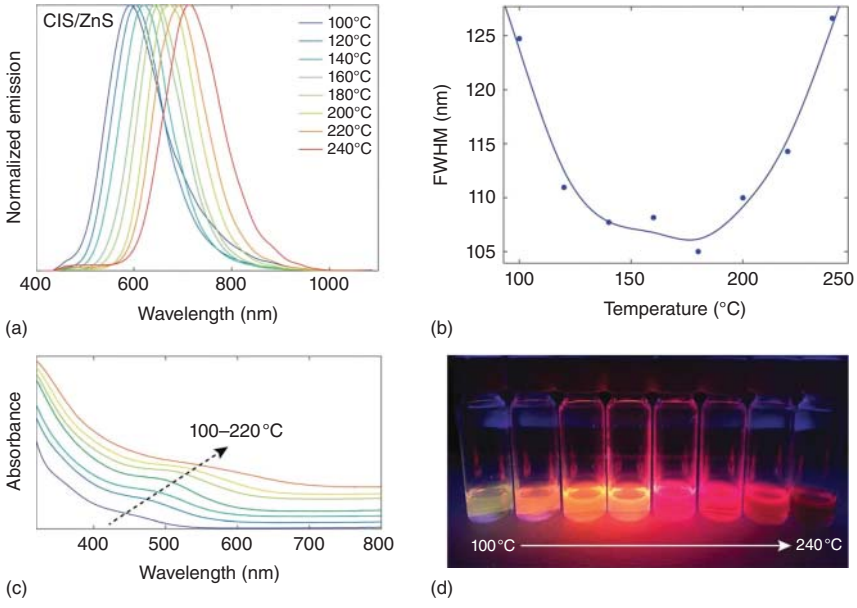

Figure 4.18 Core/shell $CuInS_2$/ZnS QDs synthesized in a two-stage droplet-based microfluidic platform. The effect of temperature within the first stage on the (a) emission spectra, (b) FWHM and (c) absorbance spectra of $CuInS_2$/ZnS QDs, and (d) $CuInS_2$/ZnS QDs (in toluene) synthesized at different temperatures within the first stage. The image was taken under UV excitation (405 nm). Source: Yashina et al. 2016 [115]. Reproduced with permission of Royal Society of Chemistry.

platform not only enabled precise dosing of reagents but also independently controlled the temperature for $CuInS_2$ core and ZnS shell formation. This feature allowed for direct tuning of the optical properties of the $CuInS_2$/ZnS QDs by changing the diameter of $CuInS_2$ cores at different reaction temperatures. As shown in Figure 4.18, PL emission maxima ranged from 580 to 760 nm and could be controlled by increasing the temperature of the first stage from 100 to 240 °C. Figure 4.18d shows an image of $CuInS_2$/ZnS QDs synthesized at different temperatures in the first stage. The authors also investigated the effect of temperature on ZnS shell formation and subsequent PL properties of $CuInS_2$/ZnS QDs. Although they tested various temperatures between 150 and 230 °C for the second stage, it was found that this did not affect the band gap of $CuInS_2$/ZnS QDs to an appreciable degree.

4.4.3 Multistep Synthesis of QDs in Segmented Flow

As an alternative to actively injecting new precursor solutions into existing droplets, it is possible to perform programmed merging of preformed droplets containing different reaction precursors. An example strategy involves the introduction of new droplets into a primary flow (via a side channel) followed by merging with incumbent droplets (Figure 4.19a). This approach requires special

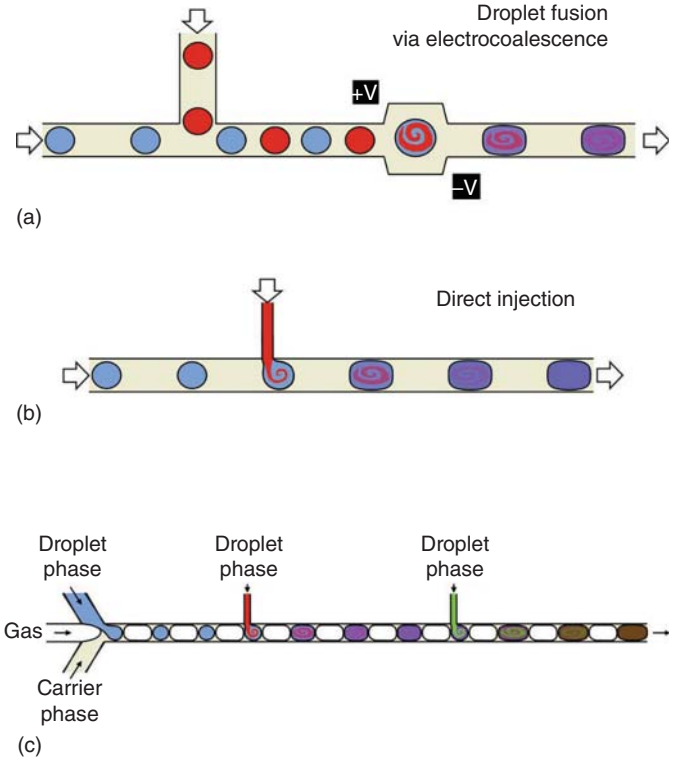

Figure 4.19 Three methods for delivering reagents into flowing droplets: (a) New reagent droplets can be introduced into a main droplet flow from the side and then merged with the native droplets by electrocoalescence; (b) direct injection of new reagent into the droplets directly from a side channel using a continuous laminar stream; (c) three-phase direct injection, where an organic solvent, a fluorous carrier, and an inert spacer gas generate a three-phase flow, and the new reagent is injected into the droplets from a side channel with a continuous flow. Source: Nightingale et al. [114]. Reproduced with permission from Nature Publishing Group.

channel architectures to bring the two droplets together [66, 116] and external electric fields to lower the interfacial tension between droplets [117–119].

Direct injection (Figure 4.19b) is generally the preferred method for droplet dosing because it does not require special channel architectures. However, there are two key challenges associated with this technique. First, it can often be challenging to obtain uniform spacing between droplets, and second, the injection volume must be minimized to prevent the (undesired) formation of new droplets from the injection stream. Both these issues can restrict the practical application of direct injection.

In an attempt to overcome the abovementioned issues, Nightingale and colleagues at Imperial College London [114] developed a three-phase droplet reactor (Figure 4.19c). The three-phase droplet flow was generated by pumping an organic solvent (ODE), a fluorous carrier (PFPE), and an inert spacer gas (argon) into a 3-to-1 flow junction, which was then fed into a PTFE capillary. Here, a

gas phase was introduced to maintain uniform droplet spacing and eliminate the possibility of generating new droplets from the side stream. Additional reagents could be injected into the flowing droplets at a T-junction, which was formed by inserting a fused silica capillary into the PTFE tubing.

The three-phase droplet reactor was used to synthesize CdSe QDs and ensure sustained particle growth (Figure 4.20). After initial droplet generation, the droplets traveled to a reaction zone for initial CdSe QD nucleation and growth within an oil bath at 233 °C. The reaction stage incorporated four T-junctions for droplet dosing via direct injection. After each dosing, the three-phase stream was pumped into a 200 °C heating zone to promote further growth. Once QD

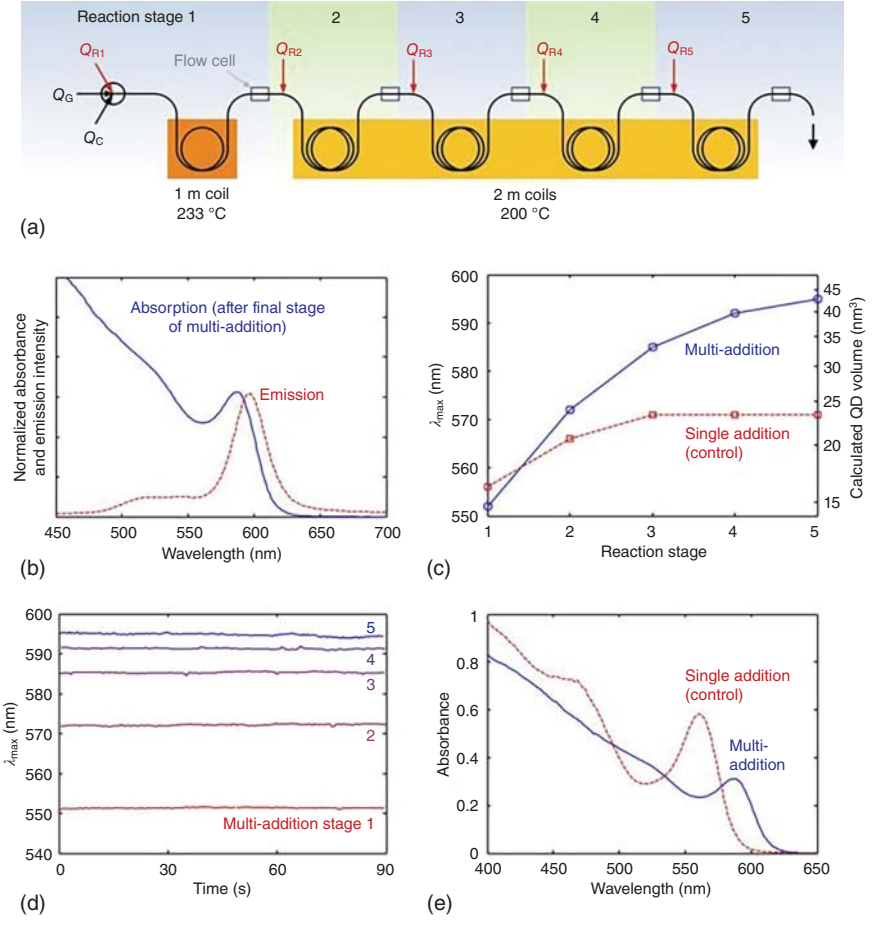

Figure 4.20 CdSe QDs synthesized by multistep droplet dosing in a three-phase droplet microreactor. (a) A schematic of a five-stage reactor for CdSe QD synthesis; (b) normalized absorption and PL spectra of the QDs after four reagent doses; (c) peak emission wavelengths for multistep and single-step precursor addition syntheses; (d) peak emission wavelengths for each of the five reaction stages during multistep synthesis; and (e) absorption spectra of the QDs from both multistep and single-step precursor addition syntheses. Source: Nightingale et al. [114]. Reproduced with permission from Nature Publishing Group.

growth was complete for each dose, the stream was cooled to room temperature before the next dosing operation. As shown in Figure 4.20d, the peak emission wavelength of the CdSe QDs exhibited a red shift with each successive growth stage, with the peak wavelength shifting from 552 to 595 nm after four droplet dosing and growth steps. To compare their multistep synthesis approach to a single injection procedure, they conducted an experiment using the same total amount of reagents but only incorporating a single addition of precursors. As shown in Figure 4.20c, the peak emission wavelength from a single addition was also red-shifted, but to a significantly lesser degree (556–571 nm).

4.4.4 Nucleation and Growth Studies of Quantum Dots

In addition to their versatility in QD synthesis, droplet microfluidic platforms are also highly effective in mechanistic studies of QD nucleation and growth when integrated with *in situ* spectroscopic characterization tools. Such an approach offers vital insight into the underlying reaction mechanisms at both short and long timescales without interfering with the reaction [120]. The three most common *in situ* spectroscopic methods are fluorescence, absorbance, and X-ray scattering (Figure 4.21).

In situ fluorescence spectroscopy is an effective and powerful characterization method for QDs as the emission peak wavelength and FWHM indicate the average size and size distribution, respectively, of the synthesized QDs [120]. Chan et al. [121] were the first to report a chip-based microfluidic reactor integrating a fluorescence detector, which they used to monitor CdSe QDs. Since this time, *in situ* fluorescence spectroscopy has commonly been integrated into microfluidic QD synthesis setups. Additionally, there are a few accounts describing the implementation of *in situ* spectroscopy to study QD nucleation and growth. An illustrative example is a report by Lignos et al. from ETH Zürich [50, 122], where they integrated both online fluorescence and absorbance spectroscopy into their droplet microfluidic platform. Figure 4.22a shows their microfluidic setup with integrated detection modules for performing online kinetic studies. The platform was fixed on an axle and a rotating movable stage, allowing measurements at different points along the reaction tubing. A light-emitting diode (LED) was used to

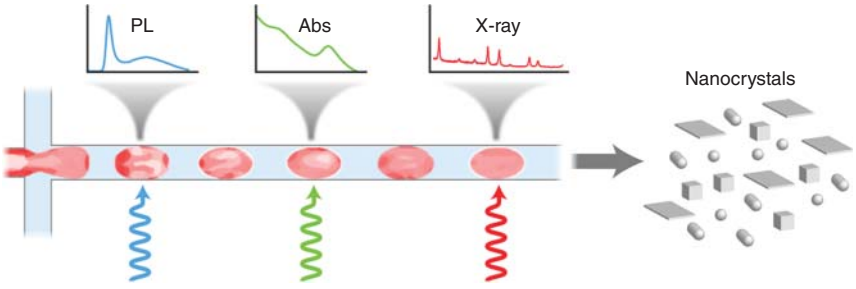

Figure 4.21 Three different *in situ* spectroscopic methods for semiconductor nanocrystal characterization. Source: Lignos et al. 2017 [50]. Reproduced with permission of American Chemical Society.

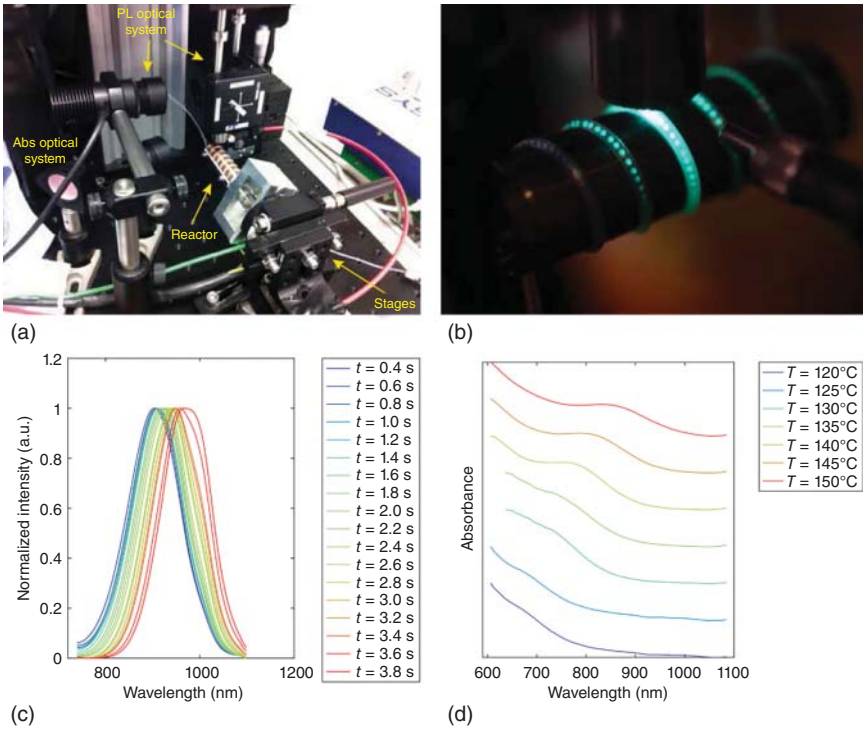

Figure 4.22 Online kinetic studies of PbS QDs. (a) an image of a microfluidic platform incorporating online absorbance and PL modules; (b) a photograph of a heating rod wrapped in capillary tubing under LED excitation; (c) PL spectrum of PbS QDs at various time points after reaction initiation; and (d) absorption spectra of PbS QDs synthesized at various temperatures. Source: Lignos et al. 2017 [50]. Reproduced with permission of American Chemical Society.

excite QDs in droplets, with emission and absorption spectra being recorded at the same time.

Such a microfluidic platform could be used for online kinetic analysis of ultra-small PbS QDs (with absorption maxima between 650 and 750 nm). Figure 4.22c shows the real-time evolution of the emission spectra at 120 °C. Interestingly, it could be seen that the position of the PL peak remained constant until 1200 ms, after which the PL peak shifted to longer wavelengths. This indicated that the size of the PbS QDs did not increase significantly during the first 1200 ms, with most of the growth occurring after this period. Figure 4.22d shows a series of absorbance spectra as a function of temperature, highlighting the maxima shift from 680 to 860 nm. The data demonstrated that the PbS QD diameters increased from 2.35 to 2.9 nm as the temperature increased from 120 to 150 °C [123]. Overall, results from this real-time absorption and PL study indicated that the mechanism of PbS QD formation comprises two steps, the first step being nucleation, where there is fast formation of PbS NPs of constant size (<1 second). This is then followed by a growth step.

4.5 Conclusions and Outlook

This chapter has provided a selective summary of some of the most important recent advances in the microfluidic synthesis of QDs, covering continuous- and segmented-flow platforms, strategies for homogenous and heterogenous QD synthesis, and integration of *in situ* monitoring techniques. It is fair to say that microfluidic technologies have already had a profound effect on our ability to synthesize high-quality QDs in a direct manner. By leveraging the advantages of microfluidics, researchers have demonstrated improvements in QD size distributions, control of reaction conditions, and QD optoelectronic properties, when compared to macroscale methods.

Despite the significant progress already achieved, there remain challenges and untapped opportunities. In the next few years, multistep methods will likely play a prominent role in the synthesis of novel and complex heterogenous nanostructures. Additionally, faster and more versatile *in situ* monitoring techniques will greatly enhance the real-time analysis of QD properties during and after synthesis. The ability to perform in-line purification is another critical technique that is needed by the end user. In-line purification is also important for multistep reactions. With each addition of reagents, unwanted chemicals (by-products, unreacted precursors, and unnecessary solvents) accumulate and affect subsequent steps in the reaction. Accordingly, successful in-line purification will greatly advance the field. Finally, large-scale production of QDs using microfluidic microreactors surprisingly remains underexplored, restricting applications in industry.

A significant opportunity exists in the coupling of microfluidic reactors with advanced control systems. The reasons for this are numerous and compelling. First, relatively complex microreactor setups will benefit significantly from automated control. Second, microfluidic reactors with integrated online and in-line characterization modules (providing real-time feedback on synthesized products) are able to generate large amounts of data, which necessitate superhuman analytical capabilities. Third, inherent problems in operating equipment for continuous syntheses (including inconsistencies in device fabrication, reactor fouling, and inefficient temperature control) can be ameliorated by intelligent monitoring systems. The use of machine learning for automated microfluidic control has already been demonstrated [124], and this will undoubtedly have a significant impact on the development of the next-generation microfluidic reactors. Finally, beyond simple control, we can envisage moving into a realm where advanced algorithms are used to map parameter spaces, study reaction products, and intelligently predict and test new compound formulations. The vast potential of this approach has already been demonstrated in QD synthesis [125]. As such, microfluidic reactor systems will offer something that not only competes with bulk synthetic approaches but also provides benefits that would otherwise be inaccessible. Accordingly, we predict that the field will progress from the regime of material synthesis and analysis into the realm of intelligent automated materials discovery, which could be truly revolutionary.

To conclude, the field of microfluidic synthesis of QDs has made enormous progress since its inception in 2002. Although there remain many challenges,

rapid developments in both nanomaterials chemistry and microfluidics will nourish the development of the field. Furthermore, it is anticipated that microfluidic synthesis tools will play a significant role in bringing QDs from promising research tools into everyday life as high-performance components in scientific and technological applications.

References

1 Whitesides, G.M. (2006). The origins and the future of microfluidics. *Nature* 442: 368–373.
2 Sun, J., Xianyu, Y., and Jiang, X. (2014). Point-of-care biochemical assays using gold nanoparticle-implemented microfluidics. *Chem. Soc. Rev.* 43: 6239–6253.
3 Mu, X., Zheng, W., Sun, J. et al. (2013). Microfluidics for manipulating cells. *Small* 9: 9–21.
4 Watts, P. and Haswell, S.J. (2005). The application of micro reactors for organic synthesis. *Chem. Soc. Rev.* 34: 235.
5 Feng, Q., Sun, J., and Jiang, X. (2016). Microfluidics-mediated assembly of functional nanoparticles for cancer-related pharmaceutical applications. *Nanoscale* 8: 12430–12443.
6 Elvira, K.S., i Solvas, X.C., Wootton, R.C.R., and Demello, A.J. (2013). The past, present and potential for microfluidic reactor technology in chemical synthesis. *Nat. Chem.* 5: 905–915.
7 Phillips, T.W., Lignos, I.G., Maceiczyk, R.M. et al. (2014). Nanocrystal synthesis in microfluidic reactors: where next? *Lab Chip* 14: 3172.
8 Hartman, R.L., McMullen, J.P., and Jensen, K.F. (2011). Deciding whether to go with the flow: evaluating the merits of flow reactors for synthesis. *Angew. Chem. Int. Ed.* 50: 7502–7519.
9 Kobayashi, J., Mori, Y., Okamoto, K. et al. (2004). A microfluidic device for conducting gas-liquid-solid hydrogenation reactions. *Science* 304: 1305–1308.
10 Efros, A.L., Rosen, M., Kuno, M. et al. (1996). Band-edge exciton in quantum dots of semiconductors with a degenerate valence band: dark and bright exciton states. *Phys. Rev. B: Condens. Matter Mater. Phys.* 54: 4843–4856.
11 Chan, W.C., Maxwell, D.J., Gao, X. et al. (2002). Luminescent quantum dots for multiplexed biological detection and imaging. *Curr. Opin. Biotechnol.* 13: 40–46.
12 Pu, Y., Cai, F., Wang, D. et al. (2018). Colloidal synthesis of semiconductor quantum dots toward large-scale production: a review. *Ind. Eng. Chem. Res.* 57: 1790–1802.
13 Darvas, F., Hessel, V., and Dormán, G. (2014). *Flow Chemistry. Volume 1, Fundamentals*. Berlin, Boston, MA: De Gruyter Textbook.
14 Susumu, K., Field, L.D., Oh, E. et al. (2017). Purple-, blue-, and green-emitting multishell alloyed quantum dots: synthesis, characterization, and application for ratiometric extracellular PH sensing. *Chem. Mater.* 29: 7330–7344.

15 Joo, D.H., Mok, J.S., Bae, G.H. et al. (2017). Colorimetric detection of Cu^{2+} and fluorescent detection of PO_4^{3-} and S^{2-} by a multifunctional chemosensor. *Ind. Eng. Chem. Res.* 56: 8399–8407.

16 Zhang, Z., Ye, Y., Pu, C. et al. (2018). High-performance, solution-processed, and insulating-layer-free light-emitting diodes based on colloidal quantum dots. *Adv. Mater.* 30: 1801387.

17 Le, T.-H., Choi, Y., Han, H. et al. (2018). Highly luminescent quantum dots in remote-type liquid-phase color converters for white light-emitting diodes. *Adv. Mater. Technol.* 3: 1800235.

18 Cho, K.-S., Lee, E.K., Joo, W.-J. et al. (2009). High-performance crosslinked colloidal quantum-dot light-emitting diodes. *Nat. Photonics* 3: 341–345.

19 He, X., Gao, L., and Ma, N. (2013). One-step instant synthesis of protein-conjugated quantum dots at room temperature. *Sci. Rep.* 3: 2825.

20 McHugh, K.J., Jing, L., Behrens, A.M. et al. (2018). Biocompatible semiconductor quantum dots as cancer imaging agents. *Adv. Mater.* 30: 1706356.

21 Zahid, M.U., Ma, L., Lim, S.J., and Smith, A.M. (2018). Single quantum dot tracking reveals the impact of nanoparticle surface on intracellular state. *Nat. Commun.* 9: 1830.

22 Takagahara, T. (1987). Excitonic optical nonlinearity and exciton dynamics in semiconductor quantum dots. *Phys. Rev. B* 36: 9293–9296.

23 Miller, D.A.B., Chemla, D.S., and Schmitt-Rink, S. (1988). Electroabsorption of highly confined systems: theory of the quantum-confined Franz–Keldysh effect in semiconductor quantum wires and dots. *Appl. Phys. Lett.* 52: 2154–2156.

24 Ivanov, S.A., Piryatinski, A., Nanda, J. et al. (2007). Type-II core/shell CdS/ZnSe nanocrystals: synthesis, electronic structures, and spectroscopic properties. *J. Am. Chem. Soc.* 129: 11708–11719.

25 Mahler, B., Lequeux, N., and Dubertret, B. (2010). Ligand-controlled polytypism of thick-shell CdSe/CdS nanocrystals. *J. Am. Chem. Soc.* 132: 953–959.

26 Gooding, A.K., Gómez, D.E., and Mulvaney, P. (2008). The effects of electron and hole injection on the photoluminescence of CdSe/CdS/ZnS nanocrystal monolayers. *ACS Nano* 2: 669–676.

27 Samanta, A., Deng, Z., and Liu, Y. (2012). Aqueous synthesis of glutathione-capped CdTe/CdS/ZnS and CdTe/CdSe/ZnS core/shell/shell nanocrystal heterostructures. *Langmuir* 28 (21): 8205–8215.

28 Drbohlavova, J., Adam, V., Kizek, R., and Hubalek, J. (2009). Quantum dots — characterization, preparation and usage in biological systems. *Int. J. Mol. Sci.* 10: 656–673.

29 Paul, M., Kettler, J., Zeuner, K. et al. (2015). Metal-organic vapor-phase epitaxy-grown ultra-low density InGaAs/GaAs quantum dots exhibiting cascaded single-photon emission at 1.3 μM. *Appl. Phys. Lett.* 106: 122105.

30 Faraday, M.X. (1857). The Bakerian Lecture. Experimental relations of gold (and other metals) to light. *Philos. Trans.* 147: 145–181.

31 Peng, Z.A. and Peng, X. (2002). Nearly monodisperse and shape-controlled CdSe nanocrystals via alternative routes: nucleation and growth. *J. Am. Chem. Soc.* 124: 3343–3353.

32 LaMer, V.K. and Dinegar, R.H. (1950). Theory, production and mechanism of formation of monodispersed hydrosols. *J. Am. Chem. Soc.* 72: 4847–4854.

33 Liu, Y. and Jiang, X. (2017). Why microfluidics? Merits and trends in chemical synthesis. *Lab Chip* 17: 3960–3978.

34 Philpot, J.S.L. (1940). The use of thin layers in electrophoretic separation. *Trans. Faraday Soc.* 35: 38.

35 Manz, A., Graber, N., and Widmer, H.M. (1990). Miniaturized total chemical analysis systems: a novel concept for chemical sensing. *Sens. Actuators, B* 1: 244–248.

36 Simpson, P.C., Woolley, A.T., and Mathies, R.A. (1998). Microfabrication technology for the production of capillary array electrophoresis chips. *Biomed. Microdevices* 1: 7–26.

37 Edel, J.B., Fortt, R., deMello, J.C., and deMello, A.J. (2002). Microfluidic routes to the controlled production of nanoparticles electronic supplementary information. *Chem. Commun.* 1136–1137.

38 Wagner, J. and Köhler, J.M. (2005). Continuous synthesis of gold nanoparticles in a microreactor. *Nano Lett.* 5: 685–691.

39 Lazarus, L.L., Riche, C.T., Marin, B.C. et al. (2012). Two-phase microfluidic droplet flows of ionic liquids for the synthesis of gold and silver nanoparticles. *ACS Appl. Mater. Interfaces* 4: 3077–3083.

40 Torigoe, K., Watanabe, Y., Endo, T. et al. (2010). Microflow reactor synthesis of palladium nanoparticles stabilized with poly(benzyl ether) dendron ligands. *J. Nanopart. Res.* 12: 951–960.

41 Abou Hassan, A., Sandre, O., Cabuil, V., and Tabeling, P. (2008). Synthesis of iron oxide nanoparticles in a microfluidic device: preliminary results in a coaxial flow millichannel. *Chem. Commun.* 1783.

42 Wang, H., Nakamura, H., Uehara, M. et al. (2002). Preparation of titania particles utilizing the insoluble phase interface in a microchannel reactor. *Chem. Commun.* 1462–1463.

43 Takagi, M., Maki, T., Miyahara, M., and Mae, K. (2004). Production of titania nanoparticles by using a new microreactor assembled with same axle dual pipe. *Chem. Eng. J.* 101: 269–276.

44 Rondeau, E. and Cooper-White, J.J. (2008). Biopolymer microparticle and nanoparticle formation within a microfluidic device. *Langmuir* 24: 6937–6945.

45 Karnik, R., Gu, F., Basto, P. et al. (2008). Microfluidic platform for controlled synthesis of polymeric nanoparticles. *Nano Lett.* 8: 2906–2912.

46 Rhee, M., Valencia, P.M., Rodriguez, M.I. et al. (2011). Synthesis of size-tunable polymeric nanoparticles enabled by 3D hydrodynamic flow focusing in single-layer microchannels. *Adv. Mater.* 23: H79–H83.

47 Khan, S.A., Günther, A., Schmidt, M.A., and Jensen, K.F. (2004). Microfluidic synthesis of colloidal silica. 20 (20): 8604–8611.

48 Wacker, J.B., Lignos, I., Parashar, V.K., and Gijs, M.A.M. (2012). Controlled synthesis of fluorescent silica nanoparticles inside microfluidic droplets. *Lab Chip* 12: 3111.

49 Nakamura, H., Yamaguchi, Y., Miyazaki, M. et al. (2002). Preparation of CdSe nanocrystals in a micro-flow-reactor. *Chem. Commun.* 2844–2845.

50 Lignos, I., Maceiczyk, R., and deMello, A.J. (2017). Microfluidic technology: uncovering the mechanisms of nanocrystal nucleation and growth. *Acc. Chem. Res.* 50: 1248–1257.

51 Nightingale, A.M. and deMello, J.C. (2010). Microscale synthesis of quantum dots. *J. Mater. Chem.* 20: 8454.

52 Song, Y., Cheng, D., and Zhao, L. (2018). *Microfluidics: Fundamental, Devices and Applications*. Wiley.

53 Wang, J. and Song, Y. (2017). Microfluidic synthesis of nanohybrids. *Small* 13: 1604084.

54 Chambers, R.D. and Spink, R.C.H. (1999). Microreactors for elemental fluorine. *Chem. Commun.* 883–884.

55 Saldanha, P.L., Lesnyak, V., and Manna, L. (2017). Large scale syntheses of colloidal nanomaterials. *Nano Today* 12: 46–63.

56 Martin, L.J., Marzinzik, A.L., Ley, S.V., and Baxendale, I.R. (2011). Safe and reliable synthesis of diazoketones and quinoxalines in a continuous flow reactor. *Org. Lett.* 13: 320–323.

57 Krishnadasan, S., Tovilla, J., Vilar, R. et al. (2004). On-line analysis of CdSe nanoparticle formation in a continuous flow chip-based microreactor. *J. Mater. Chem.* 14: 2655.

58 Marre, S., Park, J., Rempel, J. et al. (2008). Supercritical continuous-microflow synthesis of narrow size distribution quantum dots. *Adv. Mater.* 20: 4830–4834.

59 Shang, L., Cheng, Y., and Zhao, Y. (2017). Emerging droplet microfluidics. *Chem. Rev.* 117: 7964–8040.

60 Nge, P.N., Rogers, C.I., and Woolley, A.T. (2013). Advances in microfluidic materials, functions, integration, and applications. *Chem. Rev.* 113: 2550–2583.

61 Baroud, C.N., Gallaire, F., and Dangla, R. (2010). Dynamics of microfluidic droplets. *Lab Chip* 10: 2032.

62 Kintses, B., van Vliet, L.D., Devenish, S.R., and Hollfelder, F. (2010). Microfluidic droplets: new integrated workflows for biological experiments. *Curr. Opin. Chem. Biol.* 14: 548–555.

63 Boken, J., Soni, S.K., and Kumar, D. (2016). Microfluidic synthesis of nanoparticles and their biosensing applications. *Crit. Rev. Anal. Chem.* 46: 538–561.

64 Holtze, C., Rowat, A.C., Agresti, J.J. et al. (2008). Biocompatible surfactants for water-in-fluorocarbon emulsions. *Lab Chip* 8: 1632.

65 Rakszewska, A., Tel, J., Chokkalingam, V., and Huck, W.T. (2014). One drop at a time: toward droplet microfluidics as a versatile tool for single-cell analysis. *NPG Asia Mater.* 6: e133.

66 Niu, X., Gulati, S., Edel, J.B., and deMello, A.J. (2008). Pillar-induced droplet merging in microfluidic circuits. *Lab Chip* 8: 1837–1841.

67 Ahn, K., Kerbage, C., Hunt, T.P. et al. (2006). Dielectrophoretic manipulation of drops for high-speed microfluidic sorting devices. *Appl. Phys. Lett.* 88: 024104.

68 Link, D.R., Anna, S.L., Weitz, D.A., and Stone, H.A. (2004). Geometrically mediated breakup of drops in microfluidic devices. *Phys. Rev. Lett.* 92: 054503.

69 Huebner, A., Bratton, D., Whyte, G. et al. (2009). Static microdroplet arrays: a microfluidic device for droplet trapping, incubation and release for enzymatic and cell-based assays. *Lab Chip* 9: 692–698.

70 Priest, C., Herminghaus, S., and Seemann, R. (2006). Controlled electrocoalescence in microfluidics: targeting a single lamella. *Appl. Phys. Lett.* 89: 134101.

71 Tan, Y.-C. and Lee, A.P. (2005). Microfluidic separation of satellite droplets as the basis of a monodispersed micron and submicron emulsification system. *Lab Chip* 5: 1178.

72 Hatch, A.C., Patel, A., Beer, N.R., and Lee, A.P. (2013). Passive droplet sorting using viscoelastic flow focusing. *Lab Chip* 13: 1308.

73 Tan, Y.-C., Fisher, J.S., Lee, A.I. et al. (2004). Design of microfluidic channel geometries for the control of droplet volume, chemical concentration, and sorting. *Lab Chip* 4: 292.

74 Teste, B., Jamond, N., Ferraro, D. et al. (2015). Selective handling of droplets in a microfluidic device using magnetic rails. *Microfluid. Nanofluid.* 19: 141–153.

75 Abate, A.R., Agresti, J.J., and Weitz, D.A. (2010). Microfluidic sorting with high-speed single-layer membrane valves. *Appl. Phys. Lett.* 96: 203509.

76 de Ruiter, R., Pit, A.M., de Oliveira, V.M. et al. (2014). Electrostatic potential wells for on-demand drop manipulation in microchannels. *Lab Chip* 14: 883.

77 Darhuber, A.A., Valentino, J.P., and Troian, S.M. (2010). Planar digital nanoliter dispensing system based on thermocapillary actuation. *Lab Chip* 10: 1061.

78 Baroud, C.N., Robert de Saint Vincent, M., and Delville, J.-P. (2007). An optical toolbox for total control of droplet microfluidics. *Lab Chip* 7: 1029.

79 Murray, C.B., Norris, D.J., and Bawendi, M.G. (1993). Synthesis and characterization of nearly monodisperse CdE (E = S, Se, Te) semiconductor nanocrystallites. *J. Am. Chem. Soc.* 115: 8706–8715.

80 Jakeway, S.C., deMello, A.J., and Russell, E.L. (2000). Miniaturized total analysis systems for biological analysis. *Fresenius J. Anal. Chem.* 366: 525–539.

81 Lu, X., Ziegler, K.J., Ghezelbash, A. et al. (2004). Synthesis of germanium nanocrystals in high temperature supercritical fluid solvents. *Nano Lett.* 4: 969–974.

82 Holmes, J.D., Ziegler, K.J., Doty, R.C. et al. (2001). Highly luminescent silicon nanocrystals with discrete optical transitions. *J. Am. Chem. Soc.* 123: 3743–3748.

83 Eckert, C.A., Knutson, B.L., and Debenedetti, P.G. (1996). Supercritical fluids as solvents for chemical and materials processing. *Nature* 383: 313–318.

84 Kwon, B.-H., Lee, K.G., Park, T.J. et al. (2012). Continuous *in situ* synthesis of ZnSe/ZnS core/shell quantum dots in a microfluidic reaction system and its application for light-emitting diodes. *Small* 8: 3257–3262.

85 Wang, H., Li, X., Uehara, M. et al. (2004). Continuous synthesis of CdSe–ZnS composite nanoparticles in a microfluidic reactor. *Chem. Commun.* 48–49.

86 Nakamura, H., Tashiro, A., Yamaguchi, Y. et al. (2004). Application of a microfluidic reaction system for CdSe nanocrystal preparation: their growth kinetics and photoluminescence analysis. *Lab Chip* 4: 237.

87 Oh, H.J., Park, J.H., Lee, S.J. et al. (2011). Sustainable fabrication of micro-structured lab-on-a-chip. *Lab Chip* 11: 3999.

88 Becker, H. and Gärtner, C. (2008). Polymer microfabrication technologies for microfluidic systems. *Anal. Bioanal.Chem.* 390: 89–111.

89 Howes, P.D., Chandrawati, R., and Stevens, M.M. (2014). Colloidal nanoparticles as advanced biological sensors. *Science* 346: 1247390.

90 Kikkeri, R., Laurino, P., Odedra, A., and Seeberger, P.H. (2010). Synthesis of carbohydrate-functionalized quantum dots in microreactors. *Angew. Chem. Int. Ed.* 49: 2054–2057.

91 Xie, R., Rutherford, M., and Peng, X. (2009). Formation of high-quality I–III–VI semiconductor nanocrystals by tuning relative reactivity of cationic precursors. *J. Am. Chem. Soc.* 131: 5691–5697.

92 Jaffe, J.E. and Zunger, A. (1984). Theory of the band-gap anomaly in ABC_2 chalcopyrite semiconductors. *Phys. Rev. B* 29: 1882–1906.

93 Tian, S., Fu, M., Hoheisel, W., and Mleczko, L. (2016). Reaction engineering studies of the continuous synthesis of $CuInS_2$ and $CuInS_2$/ZnS nanocrystals. *Chem. Eng. J.* 289: 365–373.

94 Baek, J., Shen, Y., Lignos, I. et al. (2018). Multistage microfluidic platform for the continuous synthesis of III-V core/shell quantum dots. *Angew. Chem. Int. Ed.* 57: 10915–10918.

95 Dabbousi, B.O., Rodriguez-Viejo, J., Mikulec, F.V. et al. (1997). (CdSe)ZnS core–shell quantum dots: synthesis and characterization of a size series of highly luminescent nanocrystallites. *J. Phys. Chem. B* 101: 9463–9475.

96 Xie, R., Kolb, U., Li, J. et al. (2005). Synthesis and characterization of highly luminescent CdSe–Core CdS/Zn0.5Cd0.5S/ZnS multishell nanocrystals. *J. Am. Chem. Soc.* 127: 7480–7488.

97 Naughton, M.S., Kumar, V., Bonita, Y. et al. (2015). High temperature continuous flow synthesis of CdSe/CdS/ZnS, CdS/ZnS, and CdSeS/ZnS nanocrystals. *Nanoscale* 7: 15895–15903.

98 Shestopalov, I., Tice, J.D., and Ismagilov, R.F. (2004). Multi-step synthesis of nanoparticles performed on millisecond time scale in a microfluidic droplet-based system. *Lab Chip* 4: 316.

99 Yen, B.K.H., Günther, A., Schmidt, M.A. et al. (2005). A microfabricated gas–liquid segmented flow reactor for high-temperature synthesis: the case of CdSe quantum dots. *Angew. Chem.* 117: 5583–5587.

100 Chan, E.M., Alivisatos, A.P., and Mathies, R.A. (2005). High-temperature microfluidic synthesis of CdSe nanocrystals in nanoliter droplets. *J. Am. Chem. Soc.* 127: 13854–13861.

101 van Veggel, F.C.J.M. (2014). Near-infrared quantum dots and their delicate synthesis, challenging characterization, and exciting potential applications. *Chem. Mater.* 26: 111–122.

102 Piliego, C., Protesescu, L., Bisri, S.Z. et al. (2013). 5.2% efficient PbS nanocrystal schottky solar cells. *Energy Environ. Sci.* 6: 3054.

103 Szendrei, K., Cordella, F., Kovalenko, M.V. et al. (2009). Solution-processable near-IR photodetectors based on electron transfer from PbS nanocrystals to fullerene derivatives. *Adv. Mater.* 21: 683–687.

104 Hoogland, S., Sukhovatkin, V., Howard, I. et al. (2006). A solution-processed 1.53 μm quantum dot laser with temperature-invariant emission wavelength. *Opt. Express* 14: 3273.

105 Cao, J., Zhu, H., Deng, D. et al. (2012). *In vivo* NIR imaging with PbS quantum dots entrapped in biodegradable micelles. *J. Biomed. Mater. Res. Part A* 100A: 958–968.

106 Lignos, I., Protesescu, L., Stavrakis, S. et al. (2014). Facile droplet-based microfluidic synthesis of monodisperse IV–VI semiconductor nanocrystals with coupled in-line NIR fluorescence detection. *Chem. Mater.* 26: 2975–2982.

107 Swarnkar, A., Marshall, A.R., Sanehira, E.M. et al. (2016). Quantum dot–induced phase stabilization of α-$CsPbI_3$ perovskite for high-efficiency photovoltaics. *Science* 354: 92–95.

108 Song, J., Li, J., Li, X. et al. (2015). Quantum dot light-emitting diodes based on inorganic perovskite cesium lead halides ($CsPbX_3$). *Adv. Mater.* 27: 7162–7167.

109 Ramasamy, P., Lim, D.-H., Kim, B. et al. (2016). All-inorganic cesium lead halide perovskite nanocrystals for photodetector applications. *Chem. Commun.* 52: 2067–2070.

110 Wang, Y., Li, X., Song, J. et al. (2015). All-inorganic colloidal perovskite quantum dots: a new class of lasing materials with favorable characteristics. *Adv. Mater.* 27: 7101–7108.

111 Lignos, I., Stavrakis, S., Nedelcu, G. et al. (2016). Synthesis of cesium lead halide perovskite nanocrystals in a droplet-based microfluidic platform: fast parametric space mapping. *Nano Lett.* 16: 1869–1877.

112 Lignos, I., Protesescu, L., Emiroglu, D.B. et al. (2018). Unveiling the shape evolution and halide-ion-segregation in blue-emitting formamidinium lead halide perovskite nanocrystals using an automated microfluidic platform. *Nano Lett.* 18: 1246–1252.

113 Maceiczyk, R.M., Dümbgen, K., Lignos, I. et al. (2017). Microfluidic reactors provide preparative and mechanistic insights into the synthesis of formamidinium lead halide perovskite nanocrystals. *Chem. Mater.* 29: 8433–8439.

114 Nightingale, A.M., Phillips, T.W., Bannock, J.H., and deMello, J.C. (2014). Controlled multistep synthesis in a three-phase droplet reactor. *Nat. Commun.* 5: 3777.

115 Yashina, A., Lignos, I., Stavrakis, S. et al. (2016). Scalable production of $CuInS_2$/ZnS quantum dots in a two-step droplet-based microfluidic platform. *J. Mater. Chem. C* 4: 6401–6408.

116 Hung, L.H., Choi, K.M., Tseng, W.-Y. et al. (2006). Alternating droplet generation and controlled dynamic droplet fusion in microfluidic device for CdS nanoparticle synthesis. *Lab Chip* 6: 174.

117 Chabert, M., Dorfman, K.D., and Viovy, J.L. (2005). Droplet fusion by alternating current (AC) field electrocoalescence in microchannels. *Electrophoresis* 26: 3706–3715.
118 Frenz, L., El Harrak, A., Pauly, M. et al. (2008). Droplet-based microreactors for the synthesis of magnetic iron oxide nanoparticles. *Angew. Chem. Int. Ed.* 47: 6817–6820.
119 Mazutis, L., Baret, J.-C., Treacy, P. et al. (2009). Multi-step microfluidic droplet processing: kinetic analysis of an *in vitro* translated enzyme. *Lab Chip* 9: 2902.
120 Maceiczyk, R.M., Lignos, I.G., and deMello, A.J. (2015). Online detection and automation methods in microfluidic nanomaterial synthesis. *Curr. Opin. Chem. Eng.* 8: 29–35.
121 Chan, E.M., Mathies, R.A., and Alivisatos, A.P. (2003). Size-controlled growth of CdSe nanocrystals in microfluidic reactors. *Nano Lett.* 3: 199–201.
122 Lignos, I., Stavrakis, S., Kilaj, A., and deMello, A.J. (2015). Millisecond-timescale monitoring of PbS nanoparticle nucleation and growth using droplet-based microfluidics. *Small* 11: 4009–4017.
123 Cademartiri, L., Montanari, E., Calestani, G. et al. (2006). Size-dependent extinction coefficients of PbS quantum dots. *J. Am. Chem. Soc.* 128: 10337–10346.
124 Dressler, O.J., Howes, P.D., Choo, J., and deMello, A.J. (2018). Reinforcement learning for dynamic microfluidic control. *ACS Omega* 3: 10084–10091.
125 Bezinge, L., Maceiczyk, R.M., Lignos, I. et al. (2018). Pick a color MARIA: adaptive sampling enables the rapid identification of complex perovskite nanocrystal compositions with defined emission characteristics. *ACS Appl. Mater. Interfaces* 10: 18869–18878.